SRI International

Final Report
19 August 1994

FIELD-EMITTER ARRAYS FOR RF VACUUM MICROELECTRONICS

C.A. Spindt, Program Director
Vacuum Microelectronics Program
Physical Electronics Laboratory

SRI Project 2743

Prepared for:

Advanced Research Projects Agency
Defense Sciences Office
Virginia Square Plaza
3701 North Fairfax Drive
Arlington, VA 22203-1714

Attn: Dr. Bertram H. Hui

ARPA Order No. 8162
Contract MDA972-91-C-0029

333 Ravenswood Avenue • Menlo Park, CA 94025-3493 • (415) 326-6200 • FAX: (415) 326-5512 • Telex: 334486

Final Report
19 August 1994

FIELD-EMITTER ARRAYS FOR RF VACUUM MICROELECTRONICS

C.A. Spindt, Program Director
Vacuum Microelectronics Program
Physical Electronics Laboratory

SRI Project 2743

Prepared for:

Advanced Research Projects Agency
Defense Sciences Office
Virginia Square Plaza
3701 North Fairfax Drive
Arlington, VA 22203-1714

Attn: Dr. Bertram H. Hui

ARPA Order No. 8162

Contract MDA972-91-C-0029

Approved:

Eric Pearson, Director
Physical Electronics Laboratory

Donald L. Nielson, Vice President
Computing and Engineering Sciences Division

SRI International 333 Ravenswood Avenue • Menlo Park, CA 94025-3493 • (415) 326-6200 • FAX: (415) 326-5512 • Telex: 334486

REPORT DOCUMENTATION PAGE

Form Approved
OMB No. 0704-0188

1. AGENCY USE ONLY (Leave Blank)	2. REPORT DATE	3. REPORT TYPE AND DATES COVERED
	19 August 1994	Final Report (19 August 1991 to 30 July 1994)

4. TITLE AND SUBTITLE

Field-Emitter Arrays for RF Vacuum Microelectronics

5. FUNDING NUMBERS

6. AUTHORS

C.A. Spindt

7. PERFORMING ORGANIZATION NAME(S) AND ADDRESS(ES)

SRI International
333 Ravenswood Avenue
Menlo Park, CA 94025-3493

8. PERFORMING ORGANIZATION REPORT NUMBER

9. SPONSORING/MONITORING AGENCY NAME(S) AND ADDRESS(ES

Advanced Research Projects Agency/Defense Sciences Office
Virginia Square Plaza
3701 North Fairfax Drive
Arlington, Virginia 22203-1714

10. SPONSORING/MONITORING AGENCY REPORT NUMBER

11. SUPPLEMENTARY NOTES

12a. DISTRIBUTION/AVAILABILITY STATEMENT

Approved for public release; distribution unlimited

12b. DISTRIBUTION CODE

13. ABSTRACT *(Maximum 200 words)*

SRI International has completed a program to develop field-emitter arrays for vacuum microelectronics. We have met the first-phase program goals of 5 mA total emission, with a current density of 5 A/cm^2 for at least 2 hours and demonstrated modulation of the emission current at a frequency of 1 GHz.

Principal efforts involved the development of a process for forming emitter cones in small-diameter apertures and with improved aspect ratios to reduce stress accumulation on film, modification of reactive ion etching chemistry to eliminate sulfur contamination of the cathode, investigation of galvanic etching resulting from a deionized-water rinse, and methods of fabricating emitters arrays with increased geometric field-enhancement factors and higher packing densities.

Final efforts involved the application of small-hole lithography to low-capacitance cathode geometry, and investigation of emitter-array performance by conducting Müller microscopic imaging, Auger spectroscopy, and emission microscope measurements.

14. SUBJECT TERMS	15. NUMBER OF PAGES
Field-emitter array, vacuum microelectronics, low-capacitance cathode	75
	16. PRICE CODE

17. SECURITY CLASSIFICATION OF REPORT	18. SECURITY CLASSIFICATION OF THIS PAGE	19. SECURITY CLASSIFICATION OF ABSTRACT	20. LIMITATION OF ABSTRACT
Unclassified	Unclassified	Unclassified	Unlimited

EXECUTIVE SUMMARY

SRI International has completed Phase I of a research and development program on the SRI Spindt-type field-emitter-array cathode with a view toward eventual applications in microwave amplifiers. We have met the first-phase goals of 5 mA total emission, with a current density of 5 A/cm^2 for at least 2 hours, and demonstrated modulation of the emission current at a frequency of 1 GHz. Our approach has been to identify methods of adapting and modifying the basic cathode structure of microwave circuitry and to experimentally investigate means of implementing those methods.

During the program we have accomplished the following, as documented in detail in this final report:

- Conducted research on basic cathode technology as defined by the goals of the ARPA program and related NRL project (Section 1)
- Developed a process for forming emitter cones in small-diameter apertures (<1 μm) and with improved emitter-cone aspect ratios to reduce stress accumulation on the gate film and maintain a low capacitance, modified the reactive ion etching procedures to eliminate sulfur contamination due to the forced change in etch gas from CF_4 to SF_6, investigated galvanic etching resulting from a deionized water rinse, studied methods of fabricating emitter arrays with increased geometric field-enhancement factors (β factors) and higher packing densities, and applied small-hole lithography to low-capacitance cathode geometry (Section 2)
- Fabricated test vessels for high-frequency experiments with low-capacitance cathodes, proposed a monolithic triode structure fabricated on a diamond substrate, measured effects of an electrostatic shield integrated with the cathode, and investigated the variations in emission test results between tests on cathodes at SRI and high-frequency tests on cathodes at NRL (Section 3)
- Conducted high-frequency measurements with a triode setup to verify the program goal of modulation at 1 GHz (Section 4)
- Evaluated the effects of hydrogen plasma cleaning on cathode performance, observed the effects of plasma treatments and various gas environments, and studied emitter-array performance by conducting Müller microscopic imaging, Auger spectroscopy, and emission microscope measurements (Section 5)
- Evaluated the results of our studies and determined the feasibility of increased modulation (Section 6)

An appendix to this report lists the publications and presentations made by SRI scientists during the research program.

CONTENTS

FIGURES

1. INTRODUCTION

SRI International has participated in an effort of the Advanced Research Projects Agency (ARPA) and the Naval Research Laboratory (NRL) to perform research and development on the SRI Spindt-type field-emitter-array cathode with a view toward eventual applications in microwave amplifiers. The resulting ARPA program has been the vehicle for advancing the basic cathode technology for microwave applications (e.g., reducing intrinsic capacitance and driving voltage requirements), and has continued the original program plan to establish the characteristics of the cathode in its preprogram state of development, to identify methods of adapting and modifying the structure for microwave operation, and to experimentally investigate means of implementing those methods. For the NRL program, which began earlier than the ARPA project, SRI shifted emphasis to the support of NRL's in-house vacuum microelectronics program by providing NRL with state-of-the-art Spindt-type cathodes and consultation on setting up and using cathodes. SRI met the first-phase program goals of 5 mA total emission, with a current density of 5 A/cm^2 for at least 2 hours and demonstrated modulation of the emission current at a frequency of 1 GHz.

At the beginning of the program, two areas of development required immediate attention. The first was a materials and processing issue related to providing and maintaining a suitable vacuum environment for the cathodes. The second related to the cathode's inherent high capacitance and means for reducing that capacitance to a level that is consistent with the microwave applications envisioned for the cathode.

Our approach has been to research these two issues in parallel, using an easy-to-build, low-frequency-triode configuration fabricated on a TO-5 header as a test vehicle for materials and processing studies, and at the same time designing and researching fabrication techniques for building high-frequency-cathode structures on dielectric substrates (e.g., quartz or glass). Specific tasks addressed on these related programs have been

1. Fabrication of a supply of state-of-the-art cathodes for use in establishing cathode characteristics, and for developing structures, circuits, and procedures for testing the cathodes as triodes
2. Development of a close-spaced anode test configuration that can be used to investigate triode characteristics at low frequency (kHz to MHz) in order to study the known problems with cathode survival under close-spaced anode conditions
3. Development of a circuit for driving the cathodes and demonstrating gain, frequency response, and peak emission levels
4. Studies of advanced cathode structures (geometry, fabrication technology, and processing) for high-frequency operation

5. Investigations (with NRL) of cathode mounting and connecting procedures using practices that are consistent with the microwave goals of the effort

6. Consultations with the NRL staff on the experimental results and applications of the cathode technology

Our final effort has been directed toward improving high-frequency performance and supplying NRL with cathodes for in-house testing.

2. LOW-CAPACITANCE CATHODE FABRICATION

During 1992, the photoresist we had been using became unavailable; new resists did not hold up well to CF_4 reactive ion etching (RIE) and appeared to leave residue on the sample.

Our efforts to eliminate or remove residue from the new photoresists continued in the early part of 1993. We determined that sputter cleaning of the base film after patterning was effective in removing this residue from the base. However, sputtering of the gate was not successful because of contamination of the silicon dioxide sidewalls of the holes. In continuing cathode fabrication, we used subtle variations in processing, such as milder temperatures in the hard-bake cycle of the photoresist, so as to facilitate subsequent stripping. In addition, we found that the ovens used to bake our photoresists were not reliable with regard to maintaining set temperatures, and we felt that this could have contributed to the contamination problem.

2.1 MOLYBDENUM CONTAMINATION TESTS

We constructed a hot plate designed to bake photoresists at a reliable and repeatable temperature. Bakeout was superior to that of the previously used ovens. However, this did not eliminate the contamination problem that had been plaguing the fabrication efforts since we had to change the photoresist.

In one experiment, we noted that after the removal of the photoresist with stripper and hot phosphoric acid—which usually brightens the molybdenum—the molybdenum gate film was slightly discolored (brownish) where the photoresist for the cathode hole etch had been. We also observed that a corner of the substrate, from which the photoresist had been removed by scraping in order to make electrical contact to the gate film for electropolish etching of the holes, was not discolored.

An attempt to remove the discoloration by reactive ion etching in O_2 and CF_4 was successful. However, subsequent cleaning in hot phosphoric acid resulted in the reappearance of the discoloration everywhere but in the corner that had been scraped clean. The molybdenum was not scratched or burnished by the scraping of the resist, because the resist lifted off under the scraping action used to remove it.

Early in 1993, we began a series of controlled tests with glass and silicon substrates and a matrix of photoresist/developer/stripper combinations. Auger spectrometry measurements and depth profiling of contaminated and clean molybdenum films revealed six significant characteristics:

1. Only the 1375 photoresist produced contamination in the controlled tests.
2. Once the discoloration appeared, nothing but sputtering was able to remove it.
3. All attempts to remove the discoloration with chemicals made it worse.

4. There appeared to be no difference in results with R-10 stripper and 2001 stripper.

5. The results of these controlled tests were not always consistent with the observations made during actual cathode processing.

6. Amorphous carbon and molybdenum carbide (Mo_2C) were present on the contaminated gray-brown molybdenum film, while only amorphous carbon was present on the clean, silvery molybdenum sample.

It appeared that the problem could be the result of an ordered sequence of process steps, since our controlled step-by-step experiments had not yet produced precisely the same kind of contamination that we often encounter with the normal fabrication processes. However, our experiments, which were designed to identify the source of the problem, produced inconsistent results and were inconclusive.

By May 1993, Auger spectrometry showed that small amounts of sulfur were present on the low-frequency cathodes that were performing poorly. Sulfur has been shown to be a poison for field emission in flat-panel display applications where low-voltage sulfide-based phosphors were tried unsuccessfully. This observation was consistent with the notion of residual contamination from the new photoresists, as photoresists contain sulfur compounds. However, we noticed that a group of our standard cathodes fabricated on silicon did not show even traces of sulfur, and that they were patterned with the same resists and at about the same time as the low-capacitance cathodes.

A thorough review of the process steps of two batches of cathodes showed that the only difference was that the gate film on the low-frequency cathodes had been patterned with RIE, and the gate film of the standard cathodes had been patterned with wet chemistry. CF_4 had been previously used for our RIE of molybdenum; however, the new photoresist did not hold up well to the CF_4, so SF_6 was later used to etch the molybdenum gate film. The SF_6 is about ten times faster than the CF_4, so the new resist easily withstood the etch. We concluded that the sulfur contamination was due to the sulfur hexafluoride, but was insidious in that the sulfur did not show up on Auger spectroscopy after the etch until the photoresist had been stripped and the substrate baked.

A later series of carefully controlled tests combined with Auger spectroscopy, described in Section 2.2, positively identified the problem as being due to RIE sulfur contamination. We determined that even though the SF_6 completely etched the molybdenum well before the resist was significantly damaged, the SF_6 left a residue of sulfur on the edge of the etched molybdenum gate film under the resist where it could not be detected by the Auger spectrometer. When the substrate was heated during subsequent processing, the sulfur migrated over the entire surface of the cathode and caused erratic emission behavior and cathode failures. We thus avoided this problem by etching most of the gate pattern with the relatively fast SF_6 and then finishing the process with the CF_4, which removes the sulfur residue while completing the gate pattern etch. This two-step RIE process was adopted as our standard gate-film-patterning procedure.

Our resolution of the sulfur contamination problem enabled us to resume fabrication and testing of the low-capacitance cathodes late in May 1993. Earlier in our research, we had determined that the emitter-tip/gate geometry is a very important parameter in determining the

current/voltage characteristics of the emitter array. Generally, smaller aperture diameters and taller, sharper emitter tips are preferred for low-voltage, high-transconductance performance. Figure 1 is a scanning electron micrograph (SEM) of an early (precontamination era) emitter array that performed very well. However, later cone-formation runs using the same apparatus and procedures produced inconsistent results and less desirable cone shapes, as illustrated in Figure 2 and discussed further in Section 2.4.

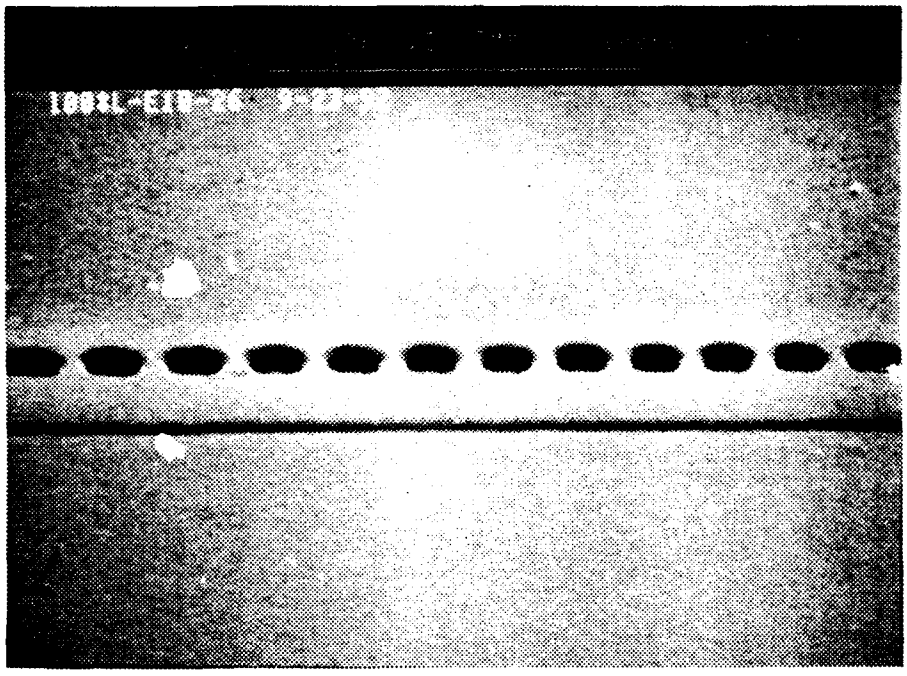

Figure 1. Scanning electron micrograph of an early low-capacitance cathode with excellent cone height and shape

2.2 AUGER SPECTROSCOPY RESULTS

Auger studies made in the summer of 1993 examined cathodes 103-E4-4S, 54E-316-1U (both of which had been tested), and 101L-A5-1B (which had not been tested). All the cathodes were stored in pinch-off tubes, and had therefore been vacuum baked.

Cathode 103-E4-4S showed a monolayer-to-submonolayer coverage of sulfur present on the surface of the gate film and gold pads. Carbon, nitrogen, and oxygen were also observed. These contaminants are to be expected following atmospheric exposure. Brief argon sputtering removed the sulfur contamination, indicating that it was present only on the surface. Subsequent depth profiling indicated that the gate film was roughly stoichiometric molybdenum carbide in the form of Mo_2C at least to a depth on the order of 100 monolayers. Profiling was not continued beyond this depth.

Cathode 54E-316-1U showed no sulfur contamination on the surface; depth profiling showed a gate film composed of Mo_2C. Cathode 101L-A5-1B had no surface sulfur contamination, but depth profiling revealed the presence of a Mo_2C gate film.

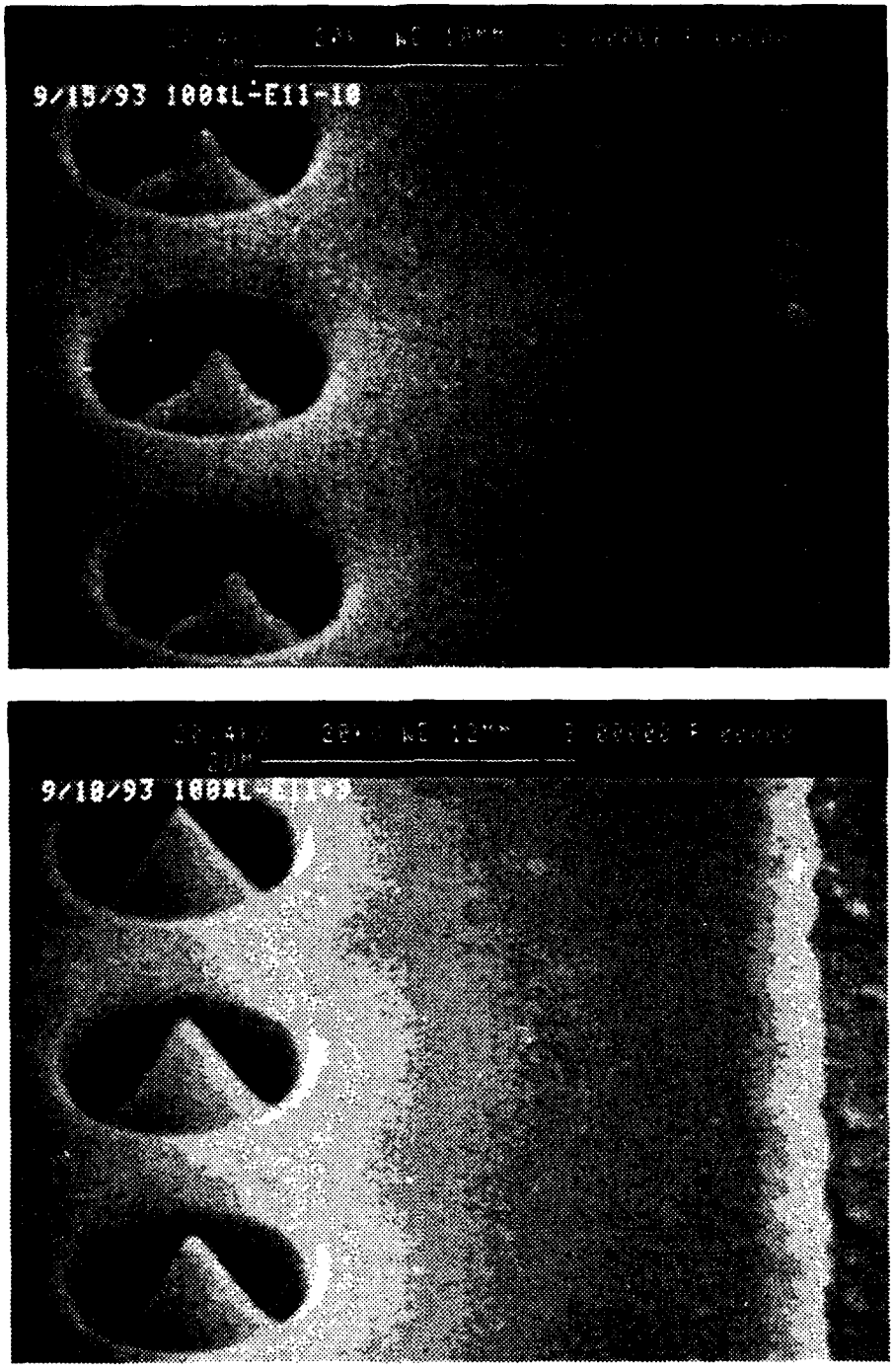

Figure 2. Scanning electron micrographs of two low-capacitance cathodes showing varying, and less than optimum, cone shapes

Because the primary difference in the three cathodes was the use of SF_6 in the preparation of the gate and base films for cathode 103-E4-4S, investigations were conducted to determine whether the SF_6 led to the sulfur contamination. We especially noted that molybdenum forms a very stable sulfide.

We conducted tests in which molybdenum films were patterned, then etched completely through with SF_6, and then with SF_6 followed by CF_4. In both cases, no sulfur was detected on the molybdenum gate or on the substrate. To investigate the possibility that the sulfur was present at the edges of the molybdenum film (it could subsequently migrate over the surface during vacuum baking at ~ 700 K), films were only partially etched through with pure SF_6 in one case, and with SF_6 followed by CF_4 in a second case. With the pure SF_6 etch, sulfur was found on the surface of the film. When the SF_6 was followed by an etch with CF_4, no sulfur was present; a small amount of fluorine was detected. Since molybdenum does not form a very stable fluoride, this was considered inconsequential.

Depth profiling again revealed both films to be composed of Mo_2C. The mobility of sulfur on Mo_2C should be very high compared to its mobility on pure molybdenum, since Mo_2C is a more stable compound than Mo_xS_y for any x and y.

2.3 SIGNIFICANCE OF MOLYBDENUM CARBIDE

The presence of Mo_2C in the gate film was very important, since the procedures and apparatus used to deposit the gate film were the same as those used to deposit the emitter cones. Thus, it appeared that our emission might have been obtained from Mo_2C rather than Mo.

The Auger electron spectroscopy observations are consistent with the general chemical behavior of the films. We noticed that the tips and gate films were not attacked by H_3PO_4. This is in agreement with the literature, which indicates that Mo is attacked by H_3PO_4, whereas Mo_2C is quite resistant to attack.

It is clearly quite important that we understand and control the extent of carbide formation, as this is critical to many performance issues, including the *enhancement* of emitter operations and reliable creation thereof. These issues are outside the scope of the present NRL and ARPA microwave cathode development programs.

2.4 FILM STRESS DURING CONE FORMATION

Cone-formation runs made late in 1993 produced relatively inconsistent results and cones, shown in the SEMs of Figure 2, that are not of our preferred geometry (tall and sharp). Cones are formed by a well-known vacuum-deposition process that is very simple in principle. The top of a micrometer-size cavity (hole) is closed by rotating the cavity while vacuum depositing material onto its top inner edge from an evaporation source positioned to deposit this material at a shallow angle relative to the surface in which the cavity is formed. While the cavity is closing, the cone is formed within it by deposition of material from a second evaporator positioned normal to the surface so that it can deposit material on the bottom of the cavity. Because of the shallow-angle source deposition, this deposited material in the cavity is formed

into a cone by the shadow-masking effect of the top inner edge of the cavity as it closes. The cone can be formed into a very sharp (~ 250 Å radius) tip if the process is done properly.

However, implementation of the process can be very demanding because several issues must be dealt with:

1. The uniformity of the holes in the gate film must be very good.
2. The cone will be too short if the hole is closed too rapidly.
3. The cone will be too tall if the hole is closed too slowly, and it will be blunt if the hole does not close completely.
4. If the ratio of deposited hole-closure material to the cone material is below a certain limit, the deposited composite film breaks up and ruins the sample.
5. If the ratio of deposited hole-closure material to the cone material is above a certain limit, the hole closes too rapidly and a poorly defined cone results.
6. If the closure film is deposited at too shallow an angle, the cone formation material forms a "hood" over the hole that is difficult or impossible to remove.
7. If the closure film is deposited at too steep an angle, the cone will be too dull.
8. The optimum closure film deposition angle depends on the hole diameter and the gate film thickness, and therefore may have to be changed for any given sample.
9. The temperature of the substrate must be within certain limits or the cone will not stick, the film may crack, or the closure film may be very difficult to etch.

To achieve a perfect cone geometry, these and other parameters must be controlled, and some of them are contradictory.

The nature of the process makes it desirable to deposit a large amount of cone-forming material onto the substrate relative to the closure material, so as to produce a tall, sharp cone. However, this is always done at the risk of breaking up the sample because of the excessive stress buildup in the deposited film.

The cone material is always metallic, and deposits with tensile stresses that can be large enough to pull underlying layers away from, or even fracture, the substrate. The chosen closure film is a material that deposits with compressive stress to help compensate for the tensile stresses of the metal film, so that thicker layers can be achieved in order to form taller, sharper cones. Historically, aluminum oxide has been used as the closure film, and molybdenum has been the cone-formation material. We have learned now to control the deposition of these materials reasonably well for our "standard" cathodes formed on silicon substrates. However, the low-capacitance configuration is formed on glass so that the base electrode can be patterned into a microstrip line. This requires that an oxide be deposited over the base and a gate layer over the oxide. The resulting structure has a "step" at the edge of the patterned base electrode, over which the composite closure and cone material film is deposited. As mentioned above, the composite film has built-in residual stresses, and any discontinuity in the surface is a "stress riser." Sharp edges are bad, and sharp corners are especially bad.

Figure 3 is a plan view of a low-capacitance cathode. The base electrode is etched with standard photolithography, which must be very precisely done because of the tolerances involved in fabricating a 4-μm-wide, 1.25-mm-long overlap with the gate electrode having a row of 1-μm-diameter holes centered along its entire length. Because of the precision of the patterning, the edge of the base film and the corners are sharp and behave as stress risers. In hindsight, it might be better to have the corners of the base rounded to reduce stress, but the sharp step along the edge is unavoidable. Other solutions are to planarize the oxide layer prior to the gate film deposition, with smaller holes so that the required thickness—and therefore the total stress in the composite layer—is reduced, or to use alternative cone materials that have less inherent stress than the molybdenum.

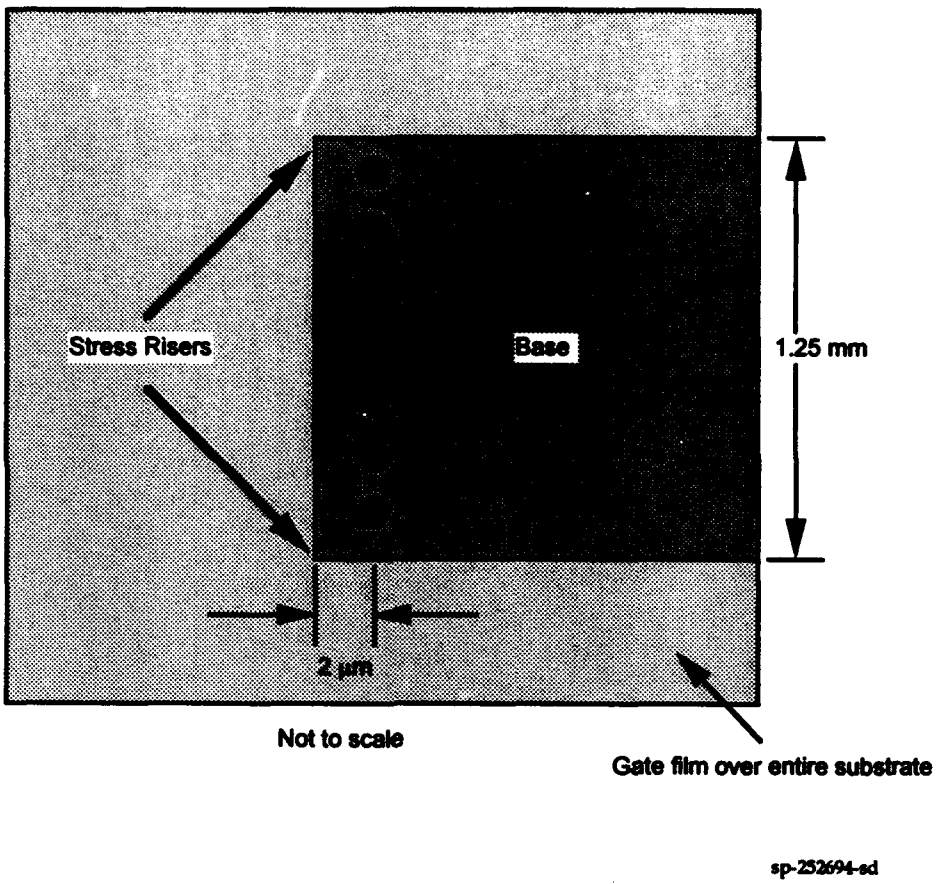

Figure 3. Point at which cracks tend to initiate in the composite closure film

Planarization can be done with a planarizing resist layer and reactive-ion etching or mechanical polishing after oxide deposition, followed by a second oxide deposition as necessary to produce the desired final oxide thickness. Alternative cone materials have some appeal in that no additional process steps would be required. In addition, the development of other cone materials may also lead to improved cone geometries because different materials naturally form taller or shorter cones, and it may also be possible to find a material with an improved work function with respect to molybdenum. Some preliminary investigations have shown that many materials—such as CR_xSi_y, Si, Nb, Cu, Th, Ni, and their combinations—are promising. The

difficulty lies in finding combinations that are compatible with the chemistry involved in the overall process, and in determining performance as a field emitter.

Some preliminary work with Cr_xSi_y produced very nice looking structures, but in emission tests the Cr_xSi_y cathodes did not perform as well as cathodes fabricated with molybdenum tips. The overcoating of a material that forms nicely shaped tips with a material that produces a preferred field-emission surface may also be an option.

2.5 GALVANIC ETCHING OF EMITTERS

Unexpected differences in gate aperture diameters from cathode to cathode across a substrate have been intermittent, and are still unexplained. Fortunately, the hole patterning has been relatively consistent in recent work. However, during our interaction with NRL we discovered an insidious and devastating effect resulting from our standard processing technique. We have routinely finished our wet-chemistry processing with a half-hour rinse in running deionized water followed by a half-hour bakeout in dry hydrogen. In the many years that we have done this, we have seen no resulting detrimental effect on the molybdenum gate or cones. On the contrary, controlled experiments showed that performance reliability was improved by this procedure as a final cleaning of the cathodes prior their being placed in our vacuum systems for testing.

Since the procedure was designed to be a final and best cleanup prior to testing, we have never done a SEM examination of the emitters after the process, because the SEM environment is not UHV clean, and past experience has shown that cathodes exposed to this environment do not perform as well as those that have not been exposed. The relevance of this is that the low-capacitance cathodes have not been inspected in the SEM after the deionized-water rinse that is done just prior to our placing the cathodes in storage/shipping vacuum vessels or into a vacuum chamber for testing.

Late in 1993, we received SEMs of cathodes that had been tested at NRL, and we were astonished to see vast differences in the emitter tips in the NRL-tested cathodes as compared to cathodes from the same batch that were tested at SRI. Figure 4 shows this effect very clearly. Figure 4a is a micrograph made at SRI of a cathode on substrate 100L-E11-22 after cone formation and before the gate patterning, dicing, and final cleanup for test. Figure 4b is a SEM made at NRL of cathode 100L-E11-22K from that substrate after gate patterning, dicing, cleaning, hydrogen firing, shipping to NRL, and testing at NRL. Clearly, there has been a change in the cones.

A step-by-step review of our process showed that the molybdenum electrodes on the low-capacitance cathodes are etched slowly during the deionized-water rinse. This appears to be the result of galvanic etching in the water. Gold contact pads have been added to the high-frequency cathode structures for bonding to microstrip lines, and the presence of the gold on the substrate apparently causes a slow galvanic dissolution of the molybdenum cones and gate in the deionized water. This etch is also rather remarkable in that the cones remain sharp, but are reduced in size as though they "shrank."

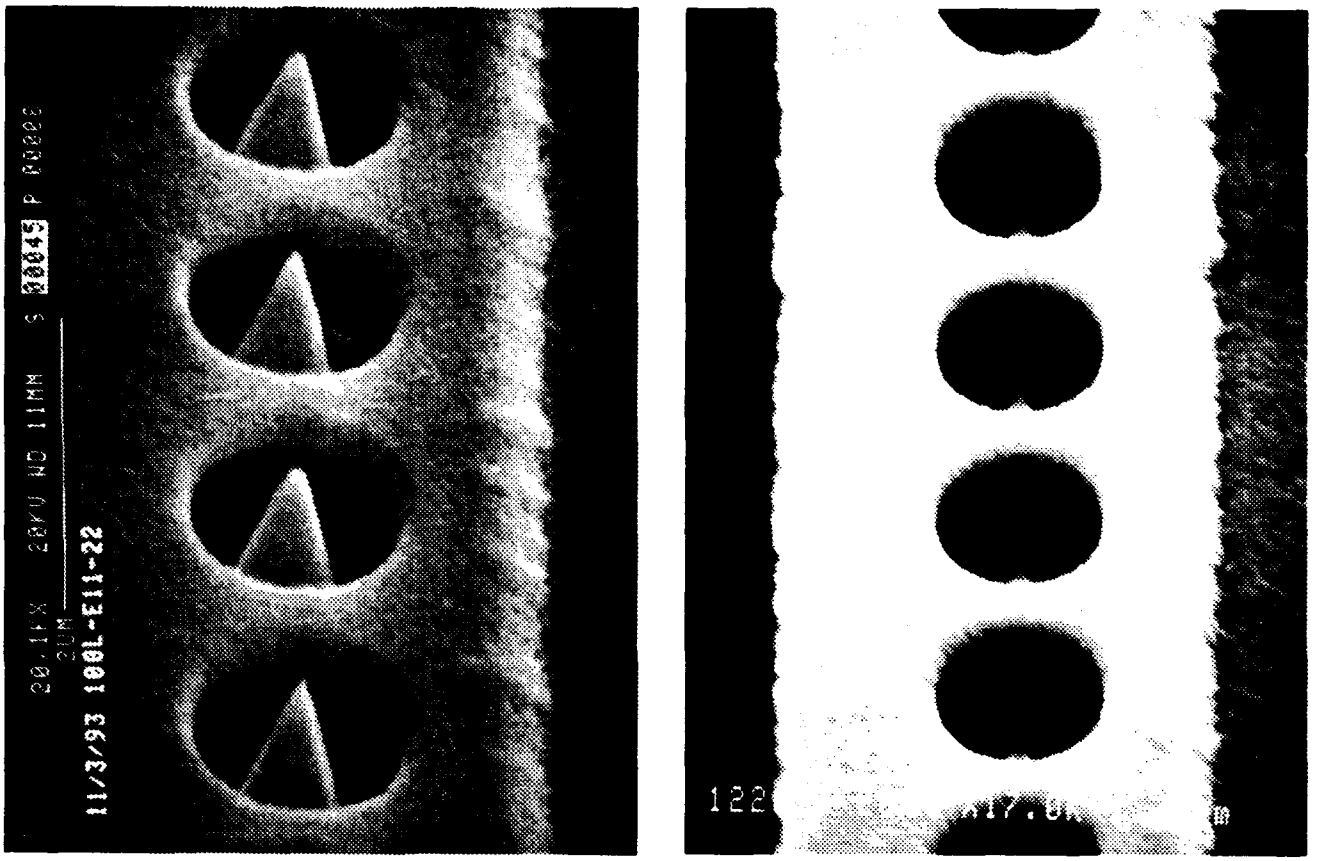

(a) (b)

sp-452094-sd

Figure 4. Scanning electron micrographs of cones from substrate 100L-E11-22: (a) at SRI as fabricated, (b) at NRL

As a confirmation of the assumption that we were dealing with a galvanic etching effect, a test cathode was monitored at each step of the process after cone formation. No change in the cone shape was detected until after a half-hour deionized-water rinse. Figure 5 illustrates the change. Figure 5a shows the cones before the deionized-water rinse, and Figure 5b shows the *same cones* viewed at the same angle and magnification after the half-hour deionized-water rinse. Etching has clearly taken place. The Figure 5 SEMs are substandard because of the gate film's being patterned prior to the microscopy, so that bare glass on the substrate charges in the electron beam and makes imaging difficult. Emitter arrays processed in the same way without gold contact pads showed no such effect. In a follow-up experiment, solvents were substituted for the deionized-water rinse of the cathodes having the gold pads, and no etching was observed.

The "half-hour" deionized-water rinse that has been used so far has not been rigorously controlled with regard to time. A half-hour was the minimum rinse time, and often the time was much longer, resulting in an even more dramatic etch of the cones. The difference in the degree to which the cones are etched in Figures 4 and 5 is most likely due to this sort of variation. It is also likely that this variation is largely responsible for the different cathode test results that have been obtained at SRI and NRL, as described in Section 3.4.

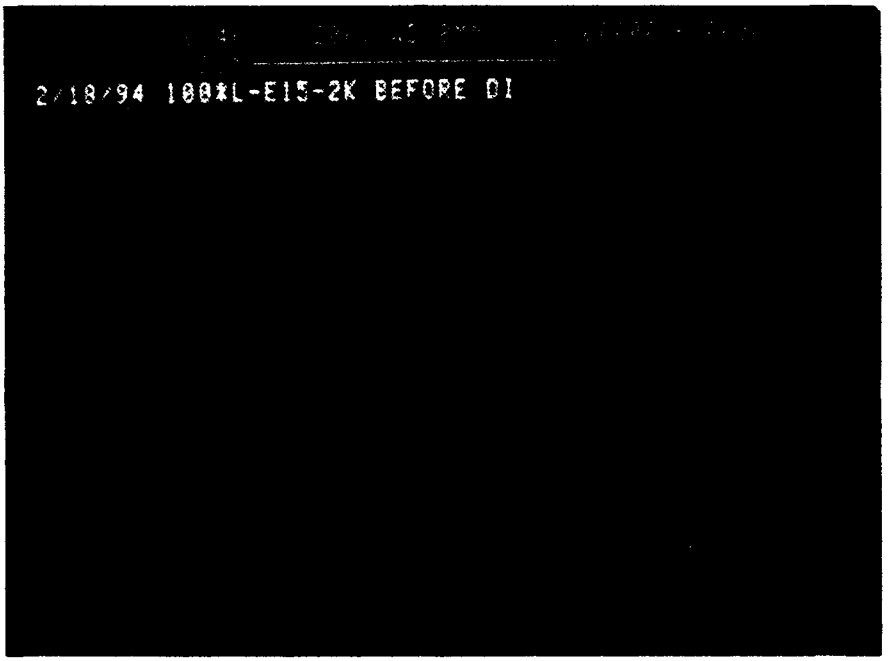

(a)

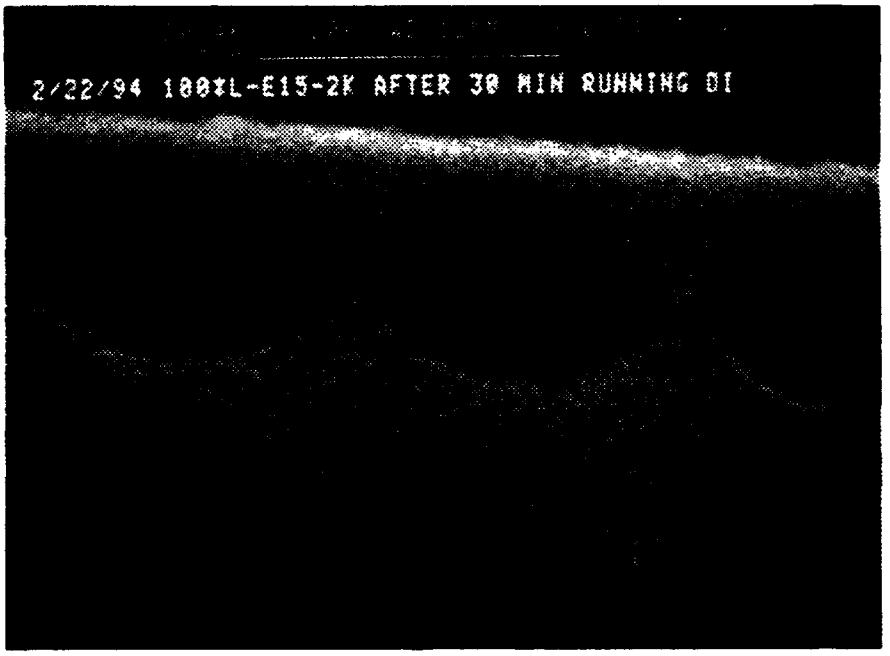

(b)

sp-552094-ed

Figure 5. Scanning electron micrographs of three emitter cones in a cathode array: (a) as fabricated, (b) same cones viewed at the same angle and magnification after a half-hour rinse in deionized water

2.6 CATHODES WITH IMPROVED β FACTOR

Studies have been under way to develop methods for fabricating emitter arrays with increased geometric field-enhancement factors (β factors) and higher packing densities, with a view toward further increasing the transconductance of the emitter arrays. Two aspects of the issue have been researched in parallel. The first is a study of ways to make smaller (submicrometer) gate aperture diameters with the goal of decreasing the voltage requirement and increasing the emitter tip packing density. The second is a study of ways of making high-aspect-ratio (cone height to base diameter), sharp cones for use with the smaller gate apertures so that it may be possible to fabricate smaller apertures and larger packing densities while maintaining the oxide thickness and capacitance. This is important, because if the capacitance is increased in the same proportion as the transconductance, the net gain in cutoff frequency is zero.

Submicrometer-hole diameters have been formed in standard SRI-supplied silicon-based test samples by Hughes Research Laboratories (HRL) using an experimental focused ion beam lithography system under development at HRL. Patterns of 100 holes in a 10×10 array have been lithographed in poly(methyl methacrylate) (PMMA) with hole diameters of approximately 1000 Å and center-to-center spacing of both 1 μm and 0.5 μm. The samples have been returned to SRI for etching and cone formation. We have also discussed acquiring small-hole samples from MIT Lincoln Laboratories.

Several samples from HRL have been processed, and significant progress has been made in our efforts to improve the cone aspect ratio. This has been done by manipulating the deposition parameters during the cone formation process. Figure 6 shows SEMs of sectioned emitters illustrating different cone aspect ratios that can be obtained by adjusting the deposition parameters during the cone formation process. The cone tip on the high aspect ratio cone is approximately 0.75 μm above the top of the gate film. Thus, it would be possible to form a well-functioning cone in a structure with 0.75-μm-thicker oxide and proportionally lower capacitance. For the same reason, it is now possible to maintain our standard oxide thickness while using much smaller gate-aperture diameters and increased tip-packing density.

The original patterns were made in cathode substrates with a 2500-Å thick oxide layer, because this work was started at the same time as investigations into means for fabricating cones with higher aspect ratios, and thus only relatively short (~ 1:1 aspect ratio) cones were originally available.

The first patterns were inadequate because of uniformity issues associated with the fact that the resist used was too thin to withstand the required etching processes. However, a double resist procedure was then used to successfully pattern holes about 0.25 μm in diameter in a 10×10 array with 1- and 0.5-μm spacing. Cones were then formed in the holes using our standard cone-forming process. Figure 7a is a SEM of one of the first 1-μm-spaced arrays made in this way, and Figure 7b is a SEM of a 0.5–μm-spaced array with cones fabricated using cone-formation processes developed to maximize the cone aspect ratio. The oxide thickness is the same in both arrays. Clearly we would be able to improve the structure by using thicker oxide and the high-aspect-ratio cones. For comparison, Figure 7c shows emitter tips from one of our standard low-capacitance cathodes with 2-μm tip spacing. The magnification is the same for all

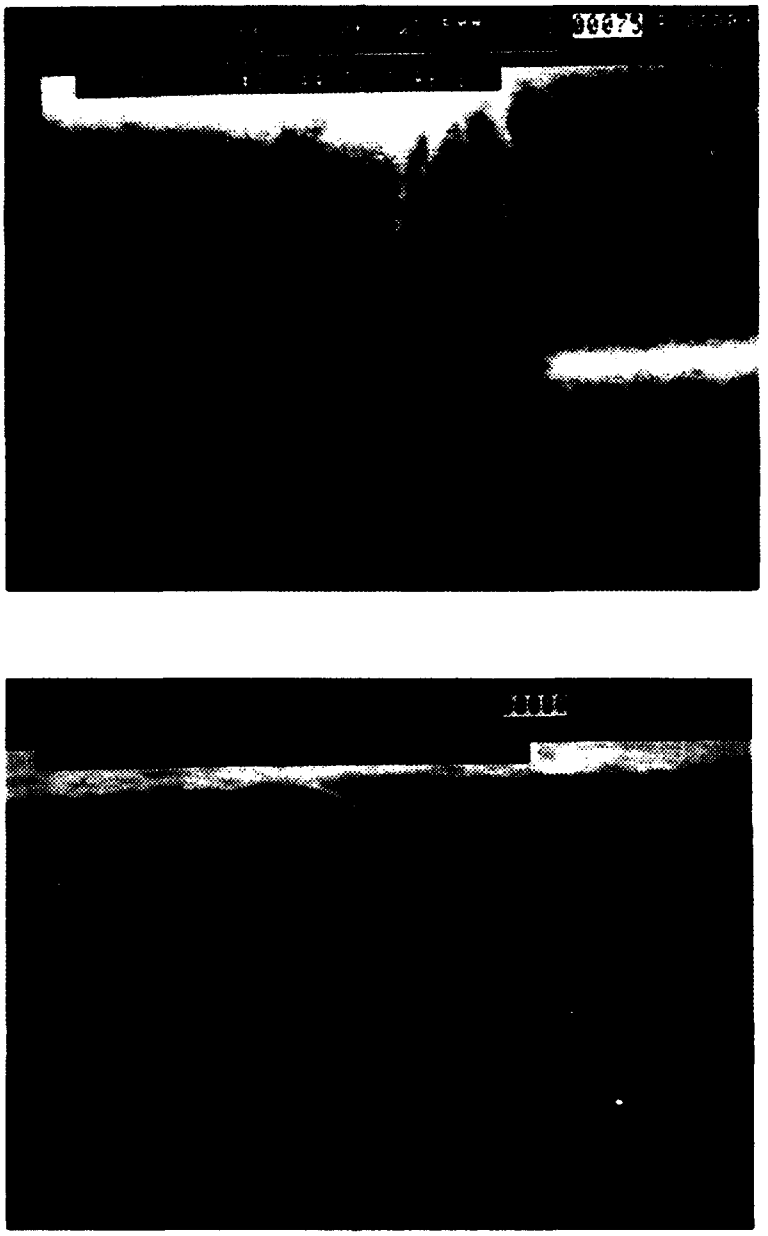

Figure 6. Scanning electron micrographs showing examples of different cone aspect ratios obtained by manipulating the deposition parameters during the cone-formation process

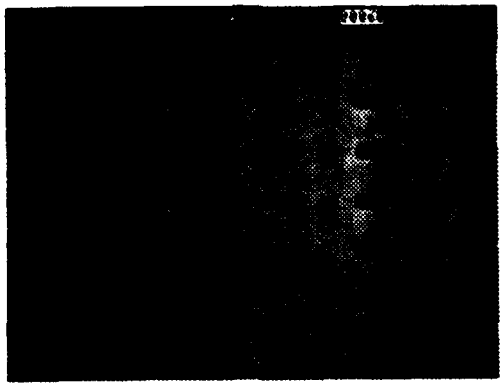

(a)

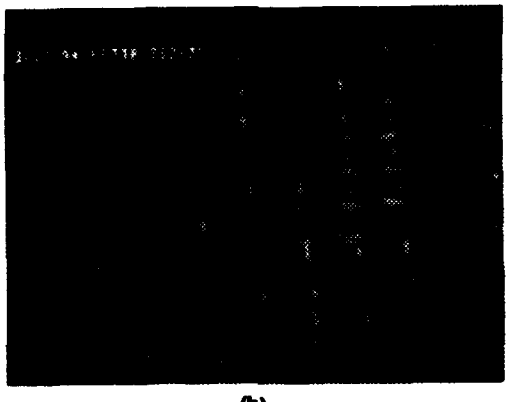

(b)

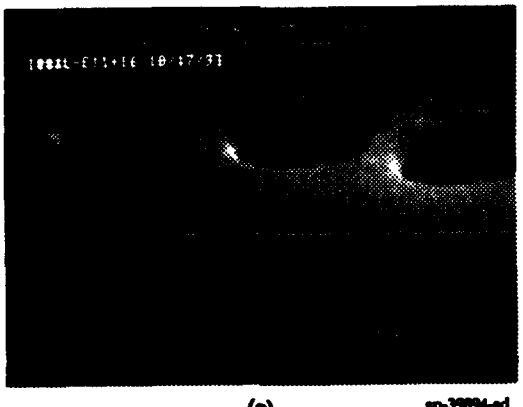

(c)

sp-39894-ed

Figure 7. Scanning electron micrographs at the same magnification of cathode arrays with gate apertures patterned with ion-beam lithography (a and b) and photolithography (c); the cathodes shown in (a and c) have standard emitter cones, and the cathode shown in (b) has high-aspect-ratio cones

three Figure 7 SEMs. The tip packing density in a 2-μm spaced array is 2.5×10^7 tips/cm^2, and for the high-density 0.5-μm spaced array it is 4×10^8 tips/cm^2.

2.7 SMALL-HOLE LITHOGRAPHY APPLIED TO THE LOW-CAPACITANCE CATHODE GEOMETRY

The team at HRL has managed to align its ion-beam pattern with the long, narrow active area of the low-capacitance cathode structure well enough to produce an acceptable yield. Figure 8 shows two SEMs. One is a portion of a low-capacitance cathode with the cones on 2-μm centers, and the other is a double row of holes on 1-μm centers etched in the molybdenum gate electrode through a PMMA resist patterned at HRL with its ion-beam lithography system. Both are the same magnification. The small hole pattern has 2500 holes in the same area as the larger pattern, which has 625 holes. When cones are formed in the small holes, the result will clearly be a higher transconductance structure due to the combination of more emitters in the cathode, and a lower operating voltage due to the higher ß factor.

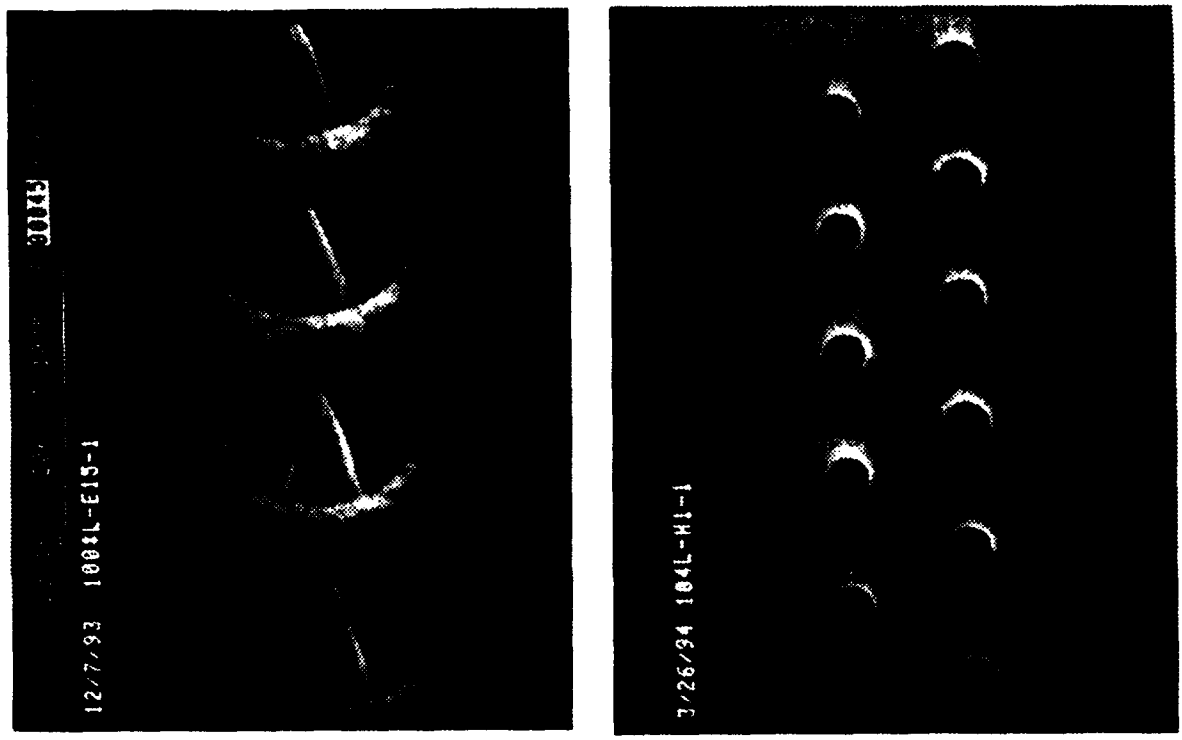

Figure 8. Scanning electron micrographs at the same magnification of low-capacitance cathodes: (a) standard structures cathode, (b) gate apertures patterned with the Hughes Ion-Beam Lithography System

3. EMISSION TESTS

The testing vessels for low-capacitance, high-frequency cathodes were completed and put on line early in 1993. Each of the two high-frequency test chambers had test sites for four cathodes.

A low-frequency qualifying chamber with test sites for six cathodes mounted in the stripline fixtures designed for microwave testing was also assembled and brought on line. We planned to qualify the cathodes in the relatively low-frequency qualifying chamber, and then transfer the best four of the six qualified cathodes into one of the high-frequency chambers. We estimated that, on the average, at least two out of three cathodes would be acceptable.

Our intention was that while a high-frequency chamber was undergoing vacuum processing, a second batch of six cathodes could be qualified in the qualifying chamber. Following this, the second high-frequency chamber would be loaded with qualified cathodes and vacuum processed while the first high-frequency chamber was undergoing high-frequency testing and the low-frequency chamber was cycled again to qualify a new batch of cathodes for the first high-frequency chamber. This sequence could be continued while improved processing and modified structures evolved from parallel fabrication and design efforts, and as we gained experience and improved our processing and measurement techniques.

In late January 1993, we could not successfully test cathodes fabricated using the new photoresists and strippers because of what turned out to be sulfur contamination. The cathodes were erratic, relatively high voltage, and tended to fail to short circuits between the base and gate at an early age. For these reasons, we discontinued testing while the contamination issue was being resolved, but we continued investigations of the basic high-frequency test configuration with regard to space charge effects on electron trajectories.

3.1 HIGH-FREQUENCY TEST CONFIGURATION

Earlier tests with low-capacitance cathodes had revealed that, compared to our standard cathode configuration, these cathodes tend to suffer from excessive gate interception of the emitted current. A study of this effect was carried out in parallel with efforts to solve the sulfur contamination problem. As a result, it was shown that the very narrow active area that is used to minimize the capacitance between the base and gate electrodes is insufficient to electrostatically shield the emitted electrons from the base electrode, as illustrated by Figure 9. The row of emitter tips is about 2 μm from the edge of the gate film, and the base electrode is, of course, below the gate and spaced about 1 μm from the gate by the silicon dioxide dielectric film.

With the edge of the gate film in such close proximity to the emitter tips, the fringing field from the base electrode deflects the emission current and causes unusually large amounts of the emission to be collected by the gate electrode. This is not a particularly surprising result, as we had previously shown that the fringing base electrode field can be used to produce a shaped

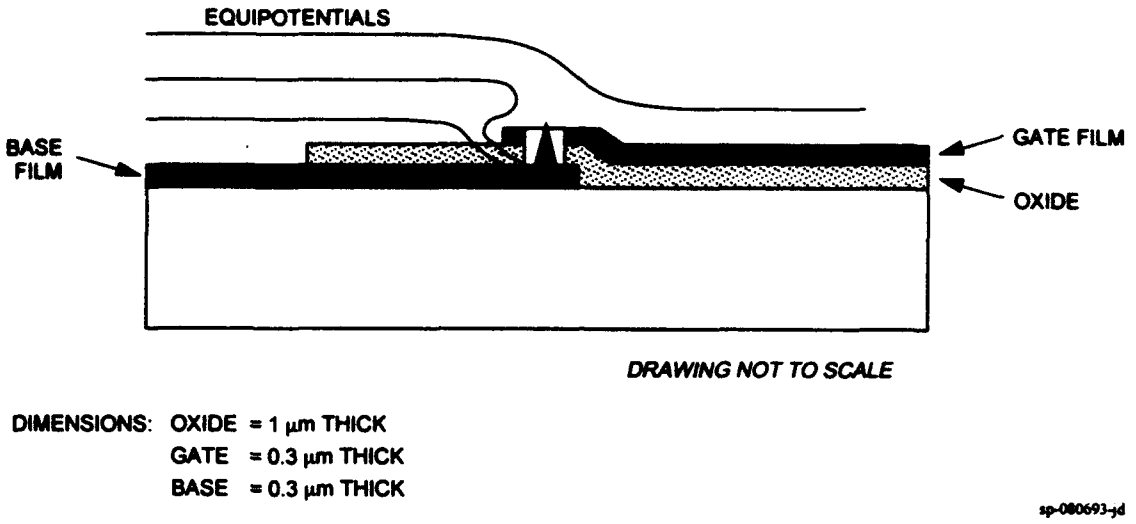

Figure 9. Cross section of the low-capacitance cathode showing the shape of the field lines in the vicinity of the active area

(focused) emission beam from a Spindt-type field emitter (Figures 10 and 11, and U.S. Patent 4,874,981). However, we did not anticipate the magnitude of the current flow that would find its way to the gate in this configuration. It appears that the beam is bent to such an extent that it allows space charge effects in the beam to shield some electrons from the influence of the anode field, with the result that these electrons return to the gate film.

In principle, placing the anode very close to the cathode could compensate for the effect of the fringing base field. However, this also has the effect of increasing capacitive coupling to the anode and increasing the power density at the anode to potentially dangerous levels. Our experience with very closely spaced anodes is that they should be avoided if possible. For this reason, we considered alternative anode configurations such as that shown in Figure 12. However, by modeling the structure, we quickly determined that, as a practical matter, the required precision of the placement of the anode for it to be effective was simply not achievable at this stage of the device development.

Because another solution for our low-capacitance geometry was necessary, we adopted the approach of shielding the active area from the base electrode by adding an electrode over the base as shown in Figure 13. The photomasks required to fabricate the structure were designed and ordered from a vendor. Figure 14 is a view of the layout of the low-capacitance cathode, showing the location of the base shield. In use, the shield would be dc biased to gate potential, but the signal would not be applied to the shield. Thus, the capacitance detected by the applied signal would not be significantly increased, but the area of the gate film would in effect be increased for the purpose of shielding the emitting area from the fringing base field.

Tests were made to determine if the relatively large area of the metal/oxide/metal structure formed by the base electrode and the shield will be a problem with respect to defect density (e.g., pinholes) in the plasma-enhanced chemical-vapor-deposited (PECVD) oxide. We found that the oxide held up well to 250 V, a higher level than that at which we expected the cathodes to have to operate.

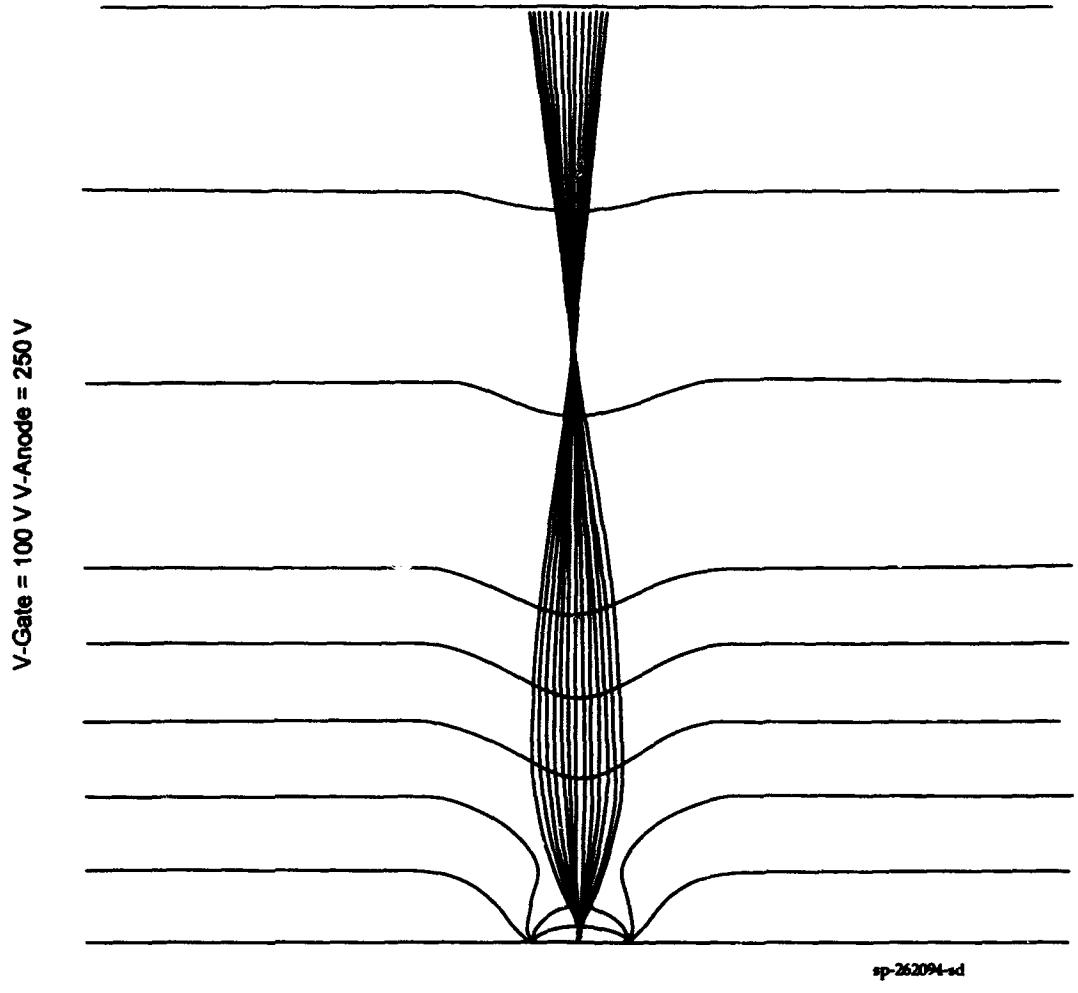

Figure 10. A computer model of trajectories from a single emitter with a small gate film area showing how the fringing fields from the base electrode can focus the beam

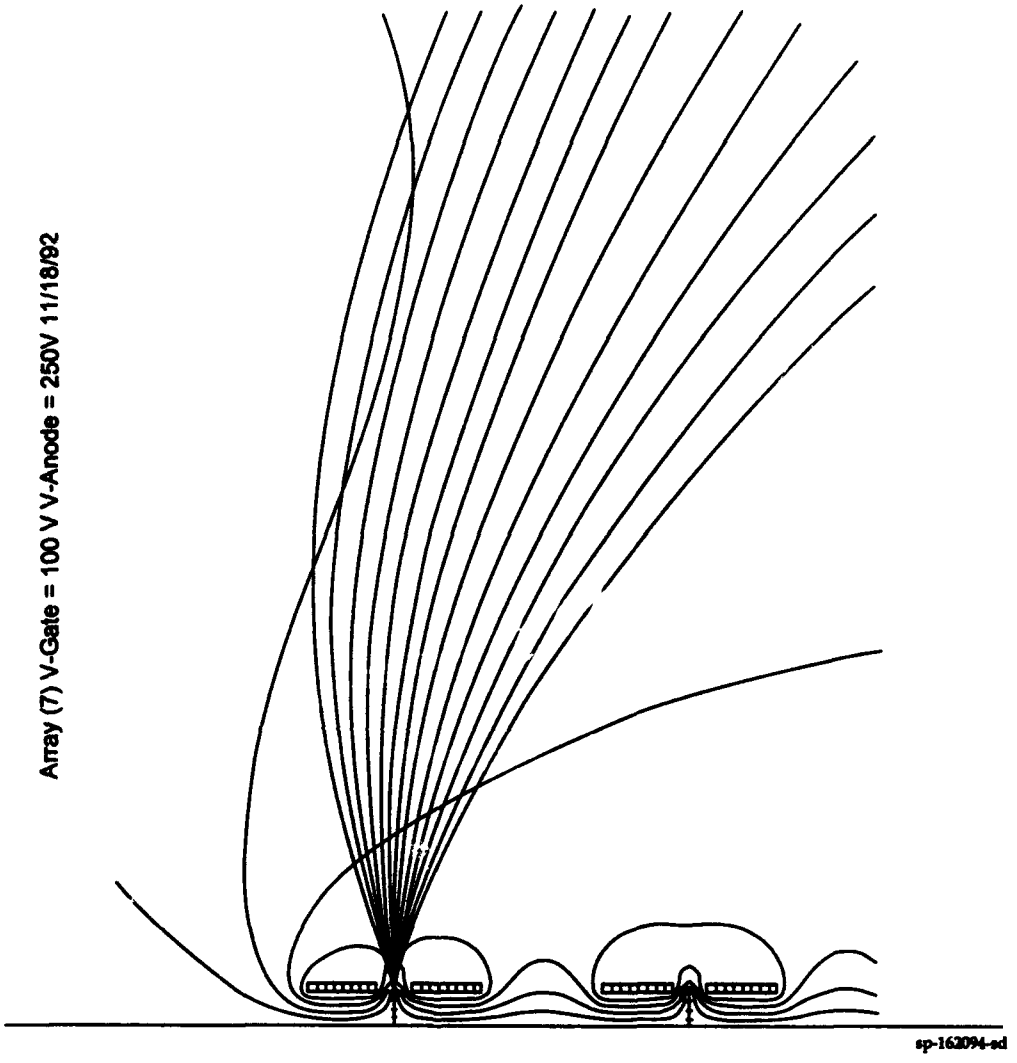

Figure 11. A computer model of trajectories from the edge of an array of Spindt-type emitters with very-small-area gate electrodes so that fringing base electrode fields influence the emitted electron beam

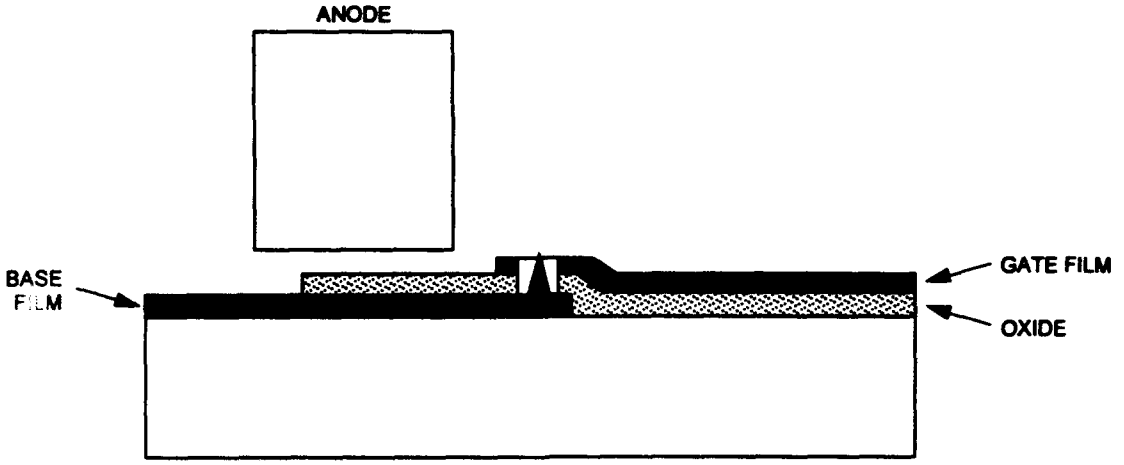

DIMENSIONS: OXIDE = 1 μm THICK
GATE = 0.3 μm THICK
BASE = 0.3 μm THICK

sp-080793-jd

Figure 12. Cross section of the low-capacitance cathode showing a desirable but impractical anode placement

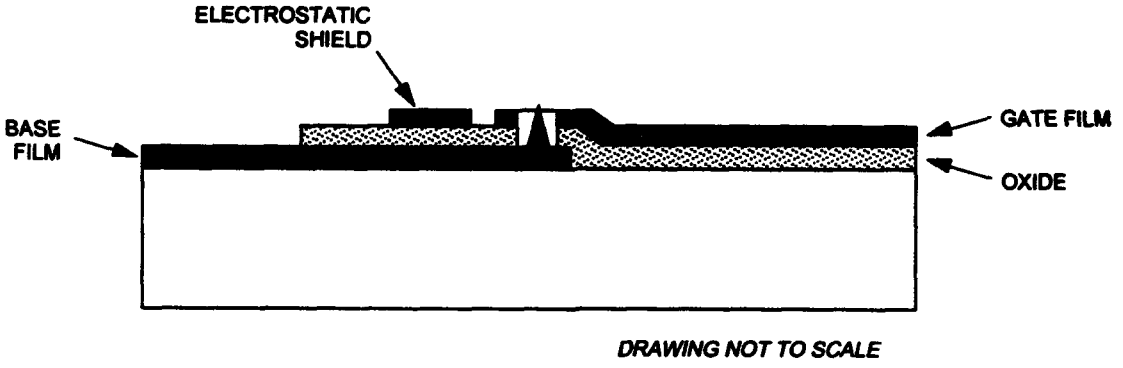

DIMENSIONS: OXIDE = 1 μm THICK
GATE = 0.3 μm THICK
BASE = 0.3 μm THICK
ELECTROSTATIC SHIELD = 0.3 μm THICK, 100 μm WIDE, 5 μm FROM THE GATE

sp-080893-jd

Figure 13. Cross section of a low-capacitance cathode showing the location of the electrostatic shield

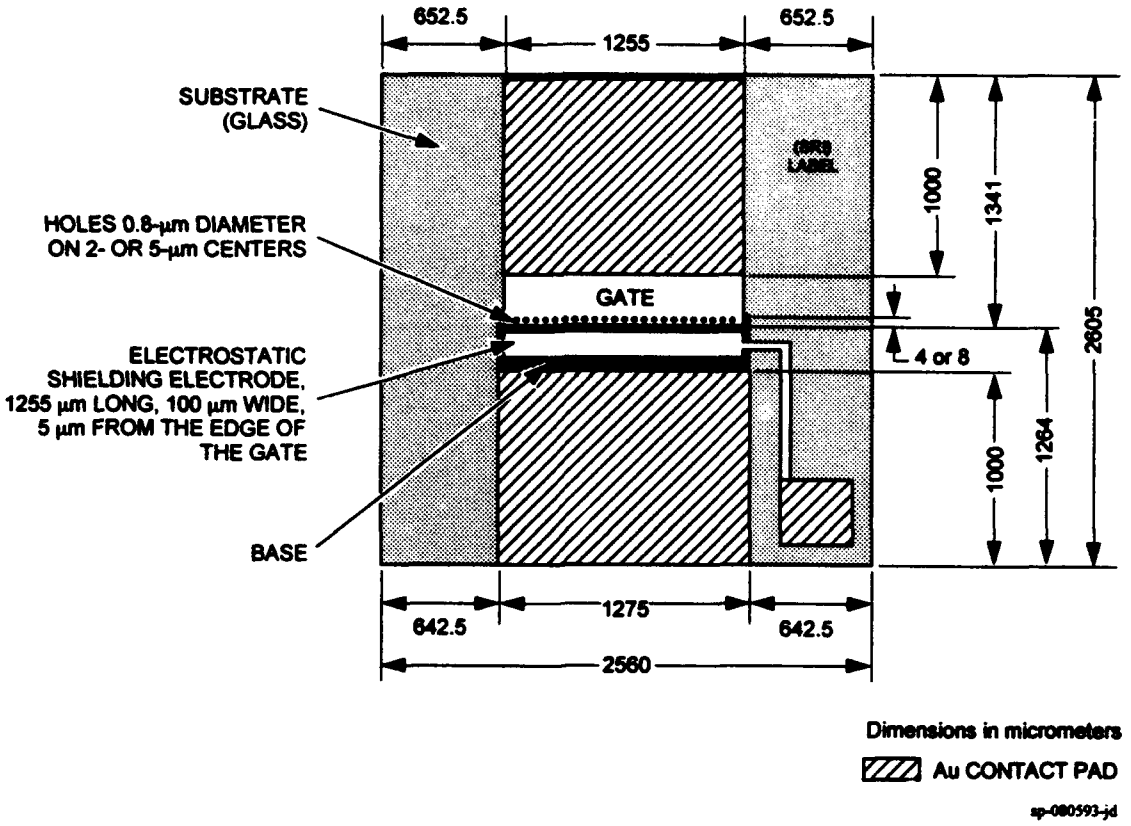

Figure 14. Layout of a low-capacitance cathode with a base shield

Careful capacitance measurements were made at NRL on cathode samples supplied by SRI to determine the shield's effects on gate capacitance. Figure 15 is a schematic diagram of the shield with the measured capacitances and the calculated capacitances based on the measurements. The results show that the shield added about 0.16 pF to the capacitance of the gate, for a total measured capacitance of 0.6 pF. This is in very good agreement with the expected gate capacitance extrapolated from measurements, made at SRI at the beginning of the program, on much larger electrode areas, using the same materials. Those results indicated that the capacitance for the high-frequency-cathode design should be in the 0.1- to 1.0-pF range, depending on the details of the hole diameters, cone geometries, oxide thickness, amount of oxide etch undercut (amount of oxide removed and replaced by vacuum), and width of the base and gate overlap area. (The overlap-area length is constant in the high-frequency configuration, and is determined by the substrate material and substrate thickness to match a 50-ohm microstrip line.)

In the summer of 1993, we fabricated and tested cathodes incorporating the shield electrode. Figure 16 shows the configuration, and Figure 17 shows the results very clearly. Figure 17a indicates the emission current and gate current with the shield electrode at base potential, and Figure 17b illustrates the same data with the shield at gate potential. The anode was at +400 V in both cases.

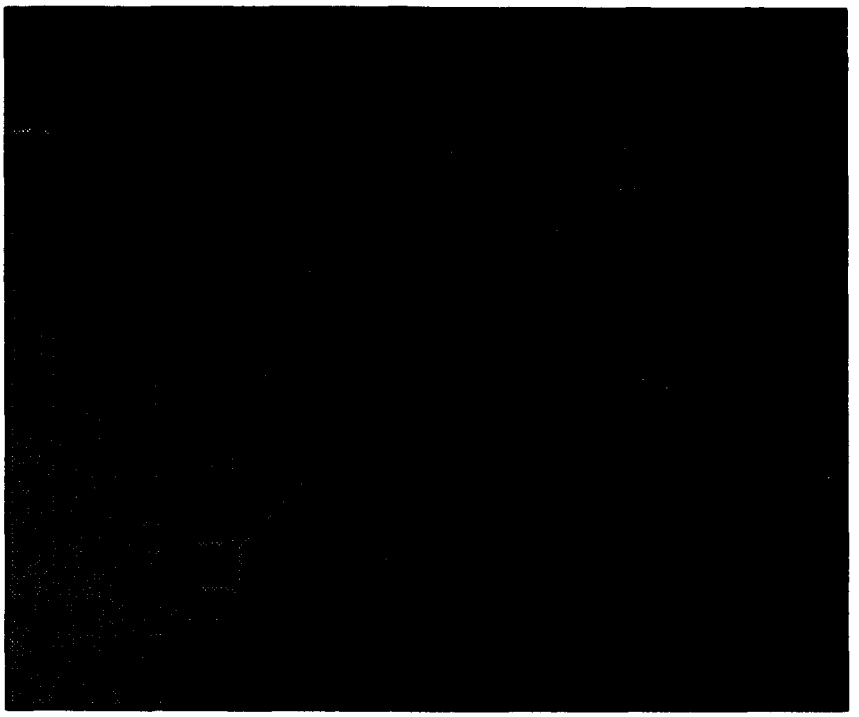

sp-652594-ad

Cgb = C3 + C1xC2/(C1+C2) = 0.60 pF

Ceb = C2 + C1xC3/(C1+C3) = 5.23 pF

Ceg = C1 + C2xC3/(C2+C3) = 0.56 pF

Cgb, Ceb, and Ceg were measured at NRL, and C1, C2, and C3 calculated as:

C1 = 0.16 pF

C2 = 5.11 pF

C3 = 0.44 pF

Figure 15. Capacitances measured at NRL

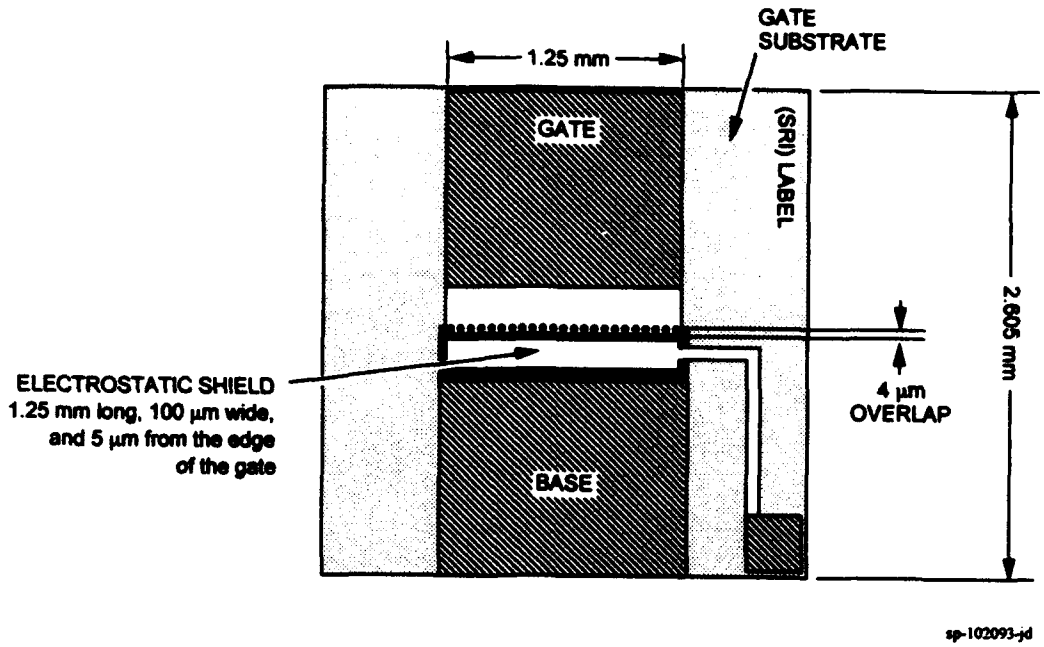

Figure 16. Schematic diagram of the location and relative size of the base shield

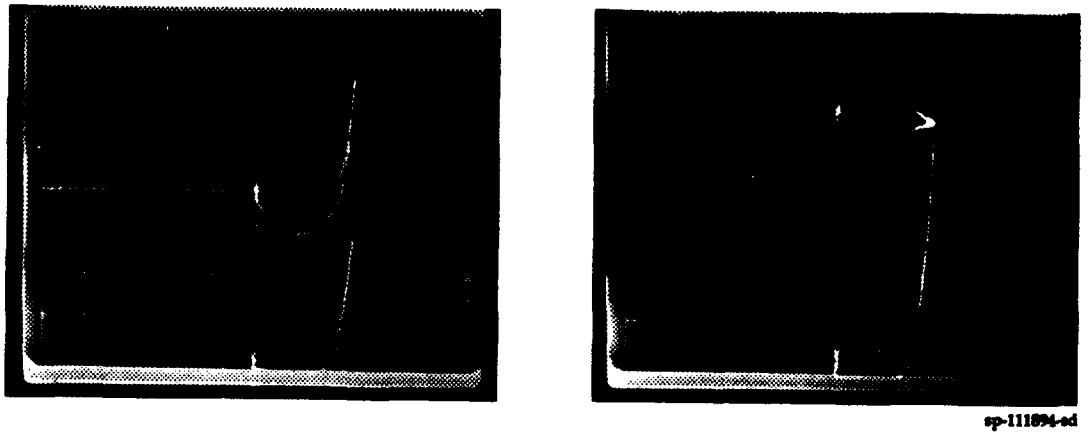

(a) With shield at base potential

(b) With shield at gate potential

Figure 17. Current/voltage curves for cathode 103L-E10+2A showing the effects of the base shield on gate current

This shield was also shown to function well as an anode, suggesting that a monolithic triode structure of the kind first described by Geppert (U.S. Patent 3,701,919: October 1973) and later reported with field-emission cathodes by Gray, Campisi, and Greene of NRL (*IDEM Digest*: 1986) might well be worth investigating with this geometry. A brief test with the shield at +160 V, anode at –22 V, tips at ground, and gate at 130 V showed that with a total emission of 100 μA, 80 μA was collected at the shield electrode. A possible triode configuration is described in Section 3.2.

3.2 PROPOSED TRIODE CONFIGURATION

A schematic diagram of a proposed monolithic triode structure fabricated on a diamond substrate is shown in Figure 18. The heat-sinking substrate was intended to result in a lead to a compact, relatively high-power triode (25 mA has been achieved; 500 V on the anode would result in a 12.4-W device). The base electrode is routed out the sides rather than under the shield to reduce capacitance; the shield is used as an anode.

The thicker anode would improve the electrostatic field distribution with respect to overcoming space charge effects in the immediate vicinity of the emitter tips, and would enhance the collection efficiency of the anode.

Figure 19 is a plan view of the proposed triode, showing the microstrip line configuration of the gate and anode electrodes and the contact pads for grounding the base electrode.

3.3 TEST RESULTS WITH SF_6 FOLLOWED BY CF_4 REACTIVE ION ETCH

After the SF_6 RIE was finished with a short CF_4 RIE to remove sulfur, CF_4 was determined to be an appropriate RIE procedure for the gate and base-shield electrodes. Emission tests were reinitiated with a new group of low-capacitance cathodes, using a group of standard cathodes (10,000 tips) on silicon as a control. Figure 20 shows the initial current/voltage characteristics at 10 μA peak emission shortly after first turn-on. The cathodes were mounted on TO-5 headers and were all in the same six-position test site, which is a standard test chamber that we have been using for several years. The chamber was baked at 700 K for 72 hours and then cooled to 350 K before the cathodes were turned on. The background pressure was in the mid 10^{-9} torr range at turn-on. The purpose was to bring the cathodes up to normal operating levels and compare their behavior. We hoped that the low-capacitance cathodes would behave in the same way as the standard cathodes, thus indicating that the contamination problem had been solved. Low-capacitance cathodes that suffered from the sulfur contamination exhibited erratic emission and, with time, a steady fall in emission level until they were no longer operational.

Emission was initiated with the test group, and brought up to 10 μA per cathode. Later, the emission was increased to 100 μA on all the cathodes. Drive voltage producing that level of emission was held constant for two weeks so that we could determine if emission would remain stable over time. We observed that emission was essentially unchanged on all six cathodes.

Figure 21 shows the current/voltage characteristics of the three low-capacitance cathodes at 10 μA peak emission after two weeks of operation at 100 μA, and the current-voltage characteristics taken at the beginning of the test period for comparison. There is very little

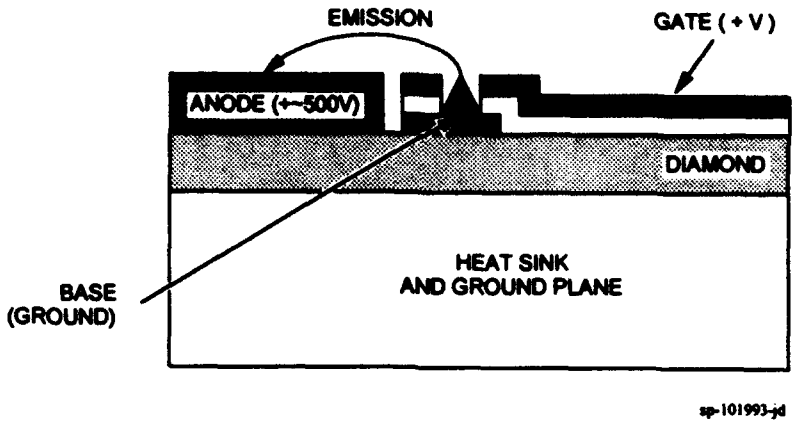

Figure 18. Monolithic triode structure on a diamond substrate with a heat sink

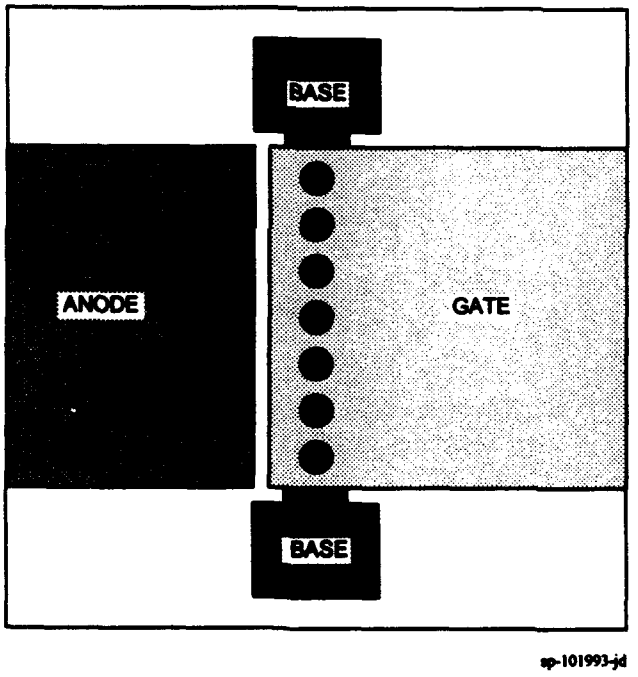

Figure 19. Plan view of a monolithic triode on a diamond heat-sink substrate

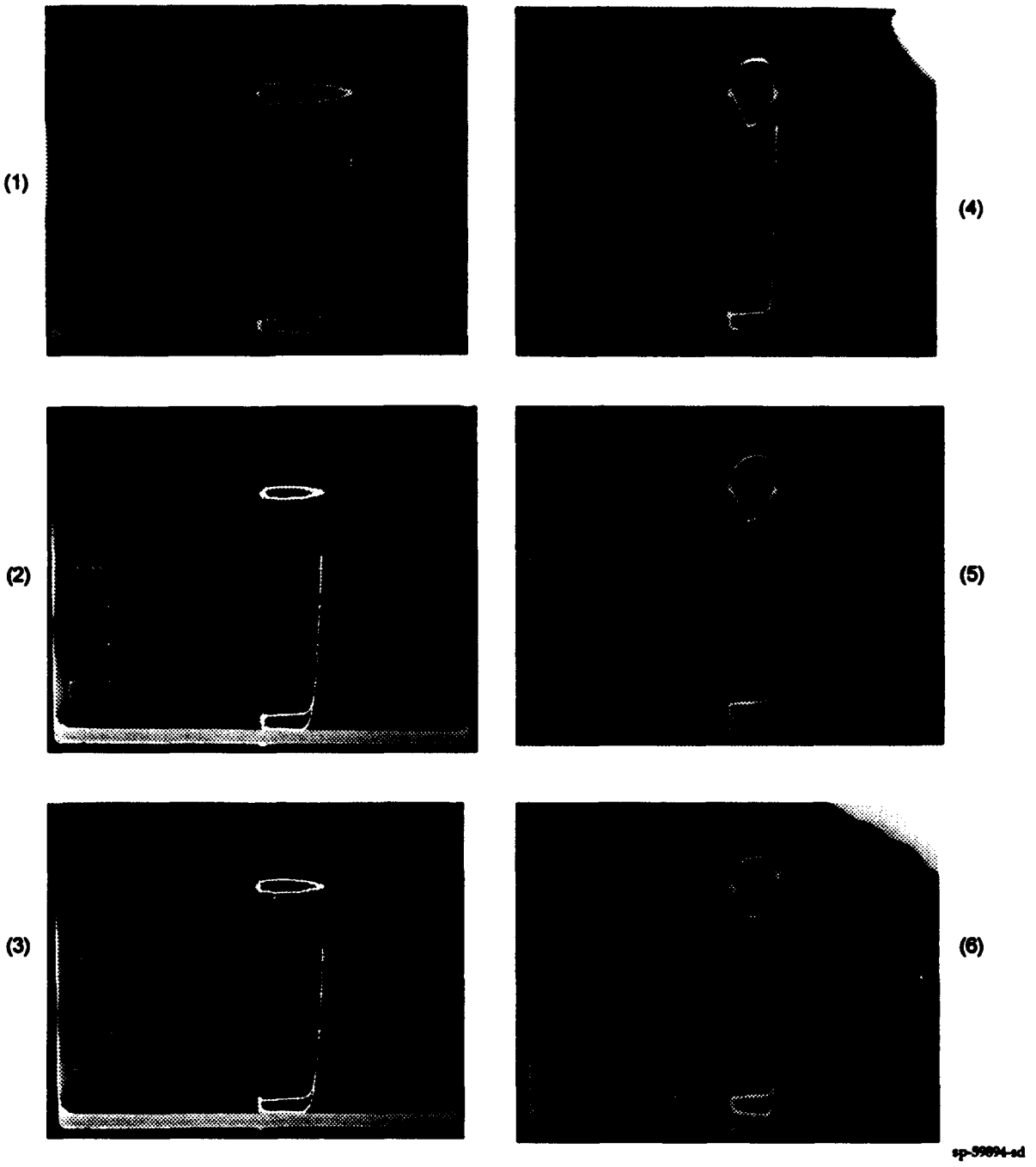

Horizontal: 50V/major division; Vertical: 5μA/major division

(1) Low-capacitance cathode 103L-E11+5B (250 tips)
(2) Low-capacitance cathode 102L-E11+5D (625 tips)
(3) Low-capacitance cathode 102L-E11+5I (625 tips)
(4) Standard cathode 52i-344-4C (10,000 tips)
(5) Standard cathode 52i-344-4D (10,000 tips)
(6) Standard cathode 52i-344-4F (10,000 tips)

Figure 20. Initial current/voltage characteristics for three low-capacitance cathodes and three standard 10,000-tip cathodes on silicon operated at the same time in the same test chamber for comparison

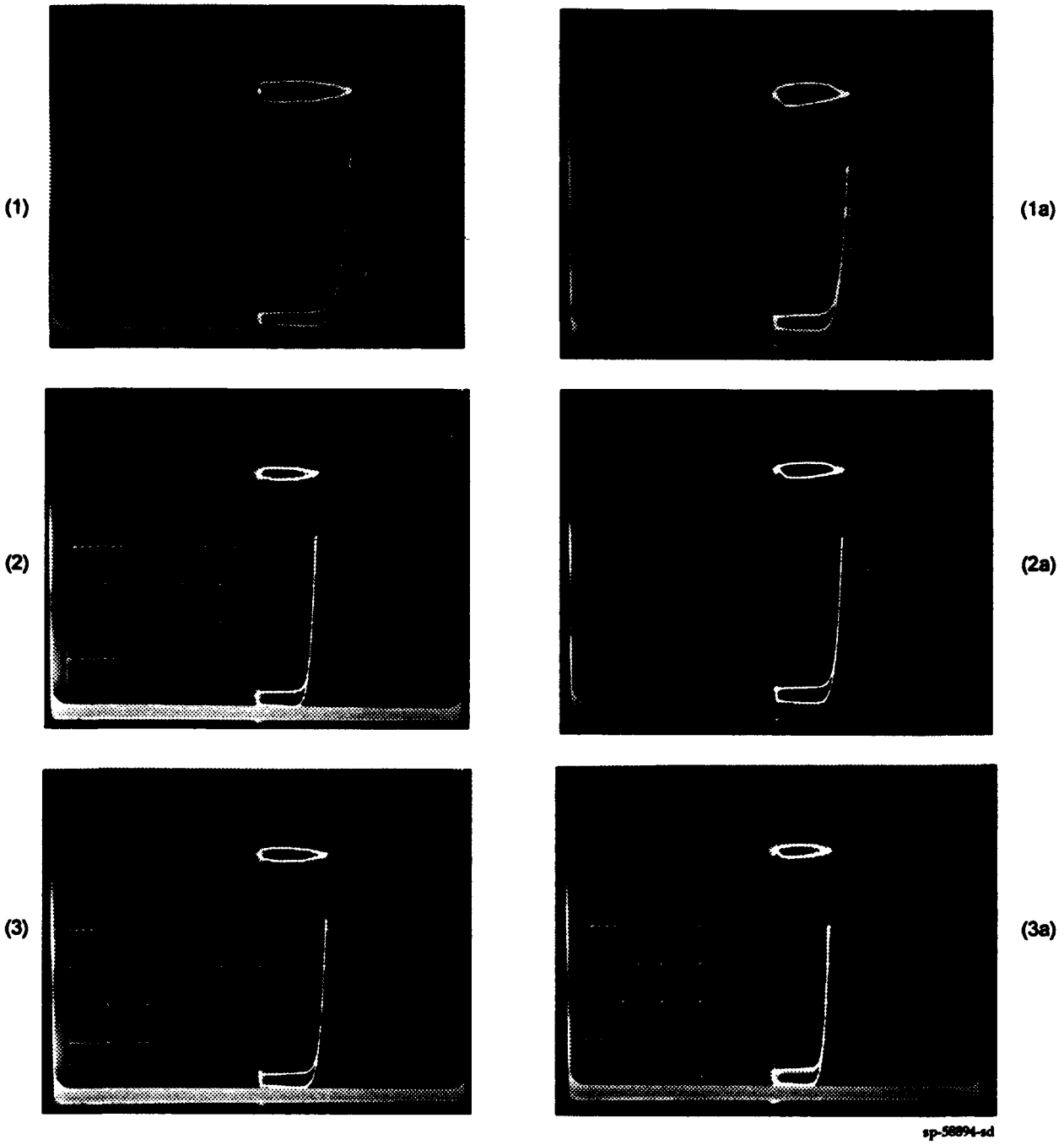

Horizontal: 50V/major division; Vertical: 5μA/major division

(1 and 1a) Low-capacitance cathode 103L-E11+5B (250 tips)
(2 and 2a) Low-capacitance cathode 102L-E11+5D (625 tips)
(3 and 3a) Low-capacitance cathode 102L-E11+5I (625 tips)

Figure 21. Current/voltage characteristics for three low-capacitance cathodes at the start of emission (1, 2, and 3), after two weeks operating at 100 μA, and then turned back to ~20 μA for comparison to the original performance (1a, 2a, and 3a)

change in the characteristics. This was encouraging evidence that the sulfur contamination problem had indeed been solved.

Late in 1993 we increased the emission level of three high-frequency cathodes under test from 100 μA to 600 μA while monitoring for signs of instability. At the 400-μA level, two of the cathodes exhibited some transient erratic gate current in the 5-μA range, and one (103L-E11+5B) required a 10-V increase in drive voltage to maintain 400 μA. The other (102L-E11+5i) did not require a perceptible increase in voltage. At the 600-μA level, cathode 103L-E11+5B was clearly damaged because a significant increase in voltage was required to maintain emission. Oscillographs of the current/voltage characteristics were taken of the three high-frequency cathodes and the three standard 10,000-tip cathodes used as controls in the experiment. The test was then terminated so that the cathodes could be examined. The oscillographs shown in Figure 22 indicate that the three 10,000-tip control cathodes (52i-344-4C, 52i-344-4D, and 52i-344-4F) were performing normally at 1-mA peak emission, each with no gate current at the time of shutdown.

Figure 23 is a Fowler-Nordheim (F/N) plot of emission data taken at shutdown. (The control cathodes are plotted as one because they were so close together that they were indistinguishable in the F/N plot.) Because the high-frequency cathodes were all made on the same substrate at the same time, it was expected that the slopes of the F/N plots would be the same and the plots would be displaced only in proportion to the number of tips in each cathode. Figure 23 shows that this is indeed the case. All three plots are essentially parallel within the limits of experimental error and the best fit of the data. The "standard" cathodes, of course, were fabricated together, but at a different time on a different substrate from the low-capacitance cathodes, and as a group have nearly identical plots but could reasonably have a different slope than the high-frequency cathodes.

The cathodes were inspected optically after removal from the test chamber. The high-frequency cathodes were of two kinds; cathode #1 had 250 emitters on 5-μm centers (103L-E11+5B), and cathodes #2 and #3 each had 625 emitters on 2-μm centers (102L-E11+5D and 102L-E11+5i, respectively). The standard control cathodes—#4, #5, and #6—were all 10,000-tip arrays on 8-μm centers. All six cathodes had approximately the same gate aperture diameters of about 1 μm.

The results of the optical inspection showed that cathode #1 had roughly half of its emitter tips blown away, cathode #2 was *totally undamaged*, and cathode #3 had nine tips blown away. Since cathode #1 had the gate apertures shown in Figure 24, it is surprising that it was working this well. It is also interesting that there is such a difference in the performance of cathodes from the same substrate.

The 10,000-tip control cathodes had very few emitter tips blown away and in such a mild fashion that it was difficult to spot them. Cathode #4 had two damaged tips, cathode #5 had six damaged tips, and cathode #6 had three damaged tips.

The large number of tips lost on cathode #1 probably explains the big difference in the level of emission between cathode #1 and cathodes #2 and #3. The difference between cathodes #2 and #3 is well within the 10% accuracy of the voltage-sensing resistors in the drive circuits used. For example, 100 μA emission was produced at 108 V and 100 V for cathodes #2 and #3,

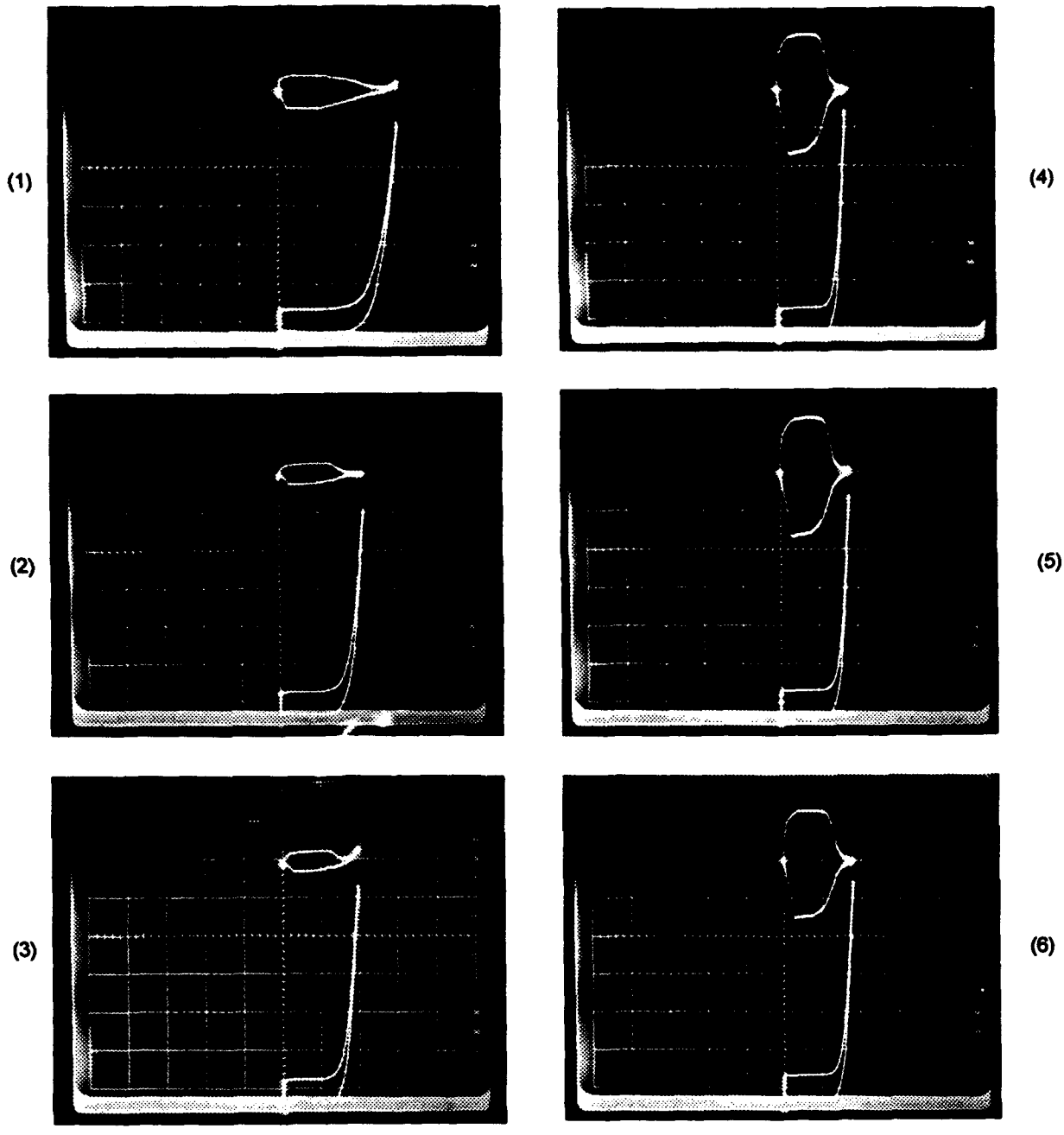

Horizontal: 50 V/major division
Vertical: 20 μA/major division

(1) Low-capacitance cathode 103L-E11+5B (250 tips)
(2) Low-capacitance cathode 102L-E11+5D (625 tips)
(3) Low-capacitance cathode 102L-E11+5i (625 tips)
(4) Standard cathode 52i-344-4C (10,000 tips)
(5) Standard cathode 52i-344-4D (10,000 tips)
(6) Standard cathode 52i-344-4F (10,000 tips)

Figure 22. Current/voltage characteristics for three low-capacitance cathodes and three standard 10,000-tip cathodes on silicon operated at the same time in the same test chamber for comparison

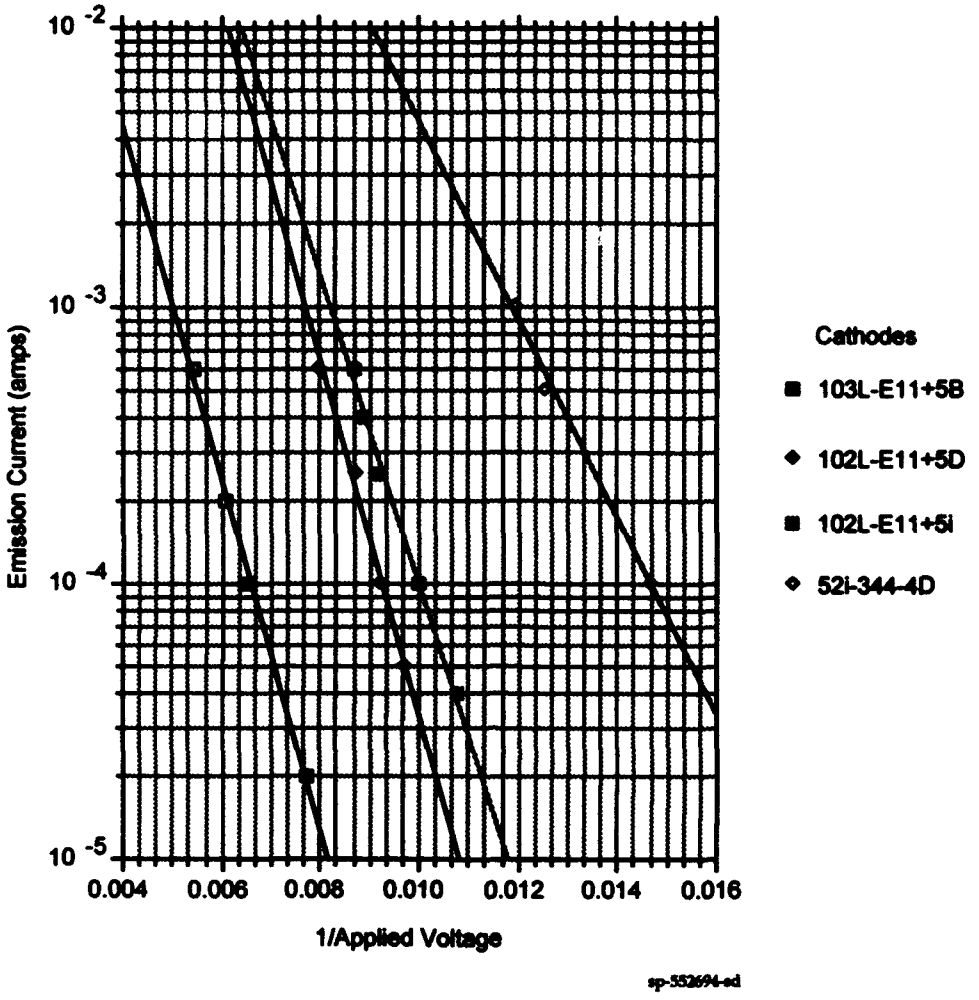

Figure 23. Fowler/Nordheim data for three high-frequency cathodes (103L = 250 tips, 102L = 625 tips) and one "standard" 10,000-tip cathode (52i)

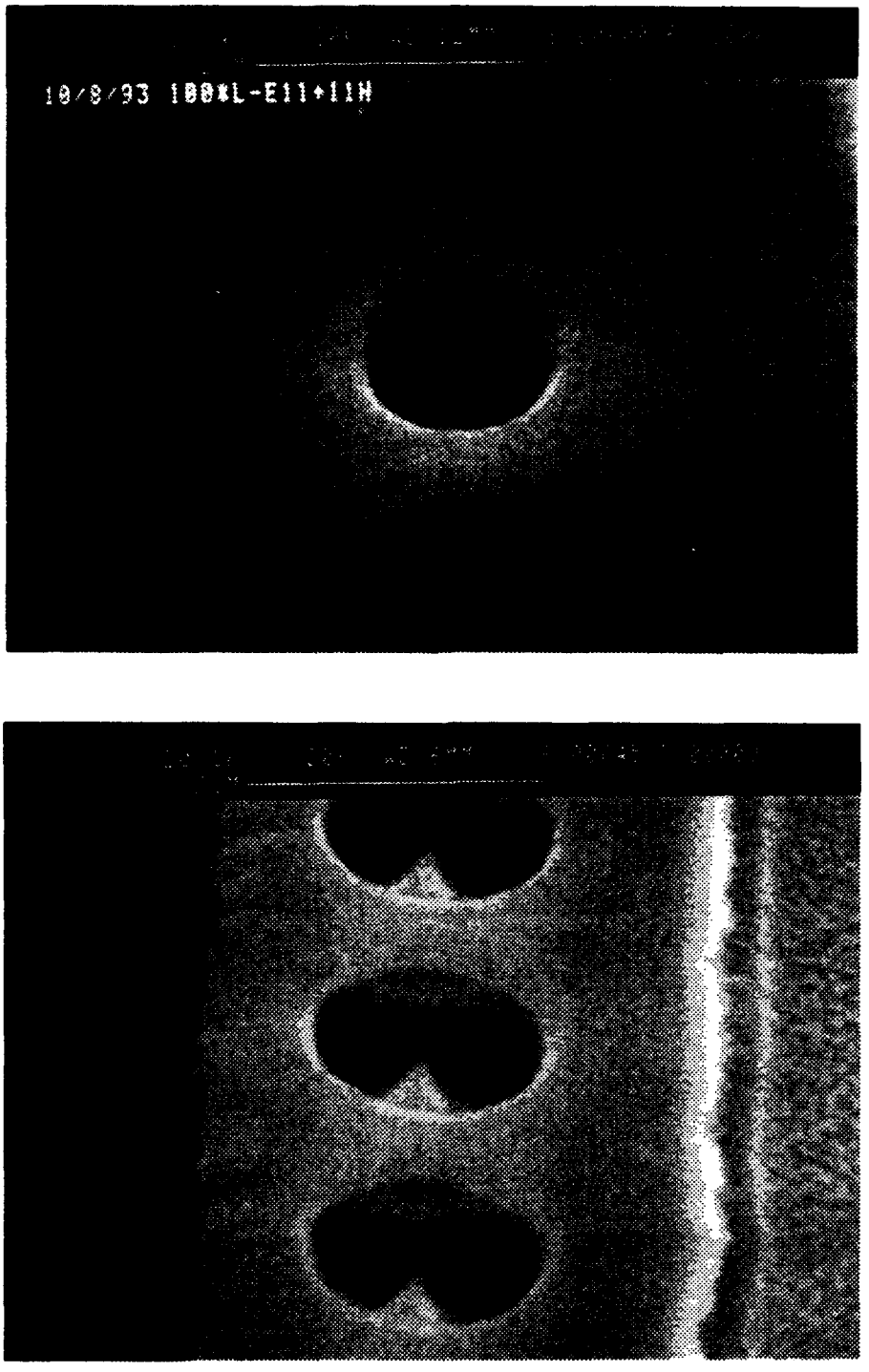

Figure 24. Scanning electron micrographs of gate apertures from opposite sides of a low-frequency cathode substrate (24 cathodes per substrate)

respectively. If the 108 V is decreased by 5% and 100 V is increased by 5%, they essentially overlap.

The overall conclusion from the tests is that the sulfur contamination problem seems to have been eliminated by the CF_4 RIE cleanup.

3.4 CATHODES TESTED AT NRL

In the fall of 1993, high-frequency cathode samples were shipped to NRL for in-house testing. Emission was obtained, but for the most part it was insufficient to permit high-frequency experiments, even with cathodes from batches that produced good results at SRI. Some of the cathodes examined at NRL showed mechanical damage that most likely occurred during the handling associated with shipping, while others were surprisingly different from what had been seen at SRI during SEM examinations of what were assumed to be representative samples from the same substrate. Normally, only a few representative samples from each substrate are examined in the SEM, because it is time-consuming and expensive (each substrate has 24 cathodes on it), and tends to leave detrimental contaminants (polymerized hydrocarbon layers) on the surfaces. It was thought that the holes on each substrate were essentially the same, and they appeared to be the same in the optical microscope, which does not have the resolution required to make accurate measurements of the hole diameters. However, it turned out that while the hole diameters were almost always the same on each cathode, they were not the same from cathode to cathode over the same substrate. The example in Figure 24 shows 1.46-μm-diameter gate apertures in cathodes on one side of the substrate and 1.13-μm-diameter apertures in cathodes on the opposite side. We were surprised by this, because the lithography is done with a state-of-the-art stepper by a local semiconductor foundry that routinely meets stringent specifications. Fortunately, this early difficulty faded away with time, and has not recurred.

In-house testing of high-frequency cathode samples at NRL early in 1994 met with limited success. Emission has been insufficient to permit high-frequency experiments. Some cathodes may have suffered mechanical damage during shipping, while others were very different from what we had seen during SEM examinations at SRI.

However, poor results compared to what had been demonstrated at SRI persisted at NRL in early 1994 until we discovered that the cathodes shipped to NRL had been damaged by galvanic etching action in the deionized-water rinse. As described in Section 2.5, as soon as we determined this etching effect, we processed three low-capacitance cathodes from each of four different substrates (24 cathodes per substrate) using alcohol instead of deionized water for the final rinse step. All twelve cathodes were then mounted in TO-5 headers and placed in our standard UHV-vacuum ion-pumped test system. The standard procedure is to rough the system with an oil-free turbomolecular pump, switch to an ion pump with a titanium sublimator at about 10^{-6} torr, and bake at 750 K for 48 hours. At the end of that time the pressure is usually about 1×10^{-9} torr, and the cathodes are turned on after the chamber is cooled to room temperature.

One of the twelve cathodes in this test had an electrical short between the base and gate electrode at turn-on, but the other eleven all produced 1 mA of emission without any difficulty. Figures 25 through 28 show current vs. voltage data for the eleven cathodes that worked well. The spread in the data within each group occurs because some cathodes have 250 tips on 5-μm

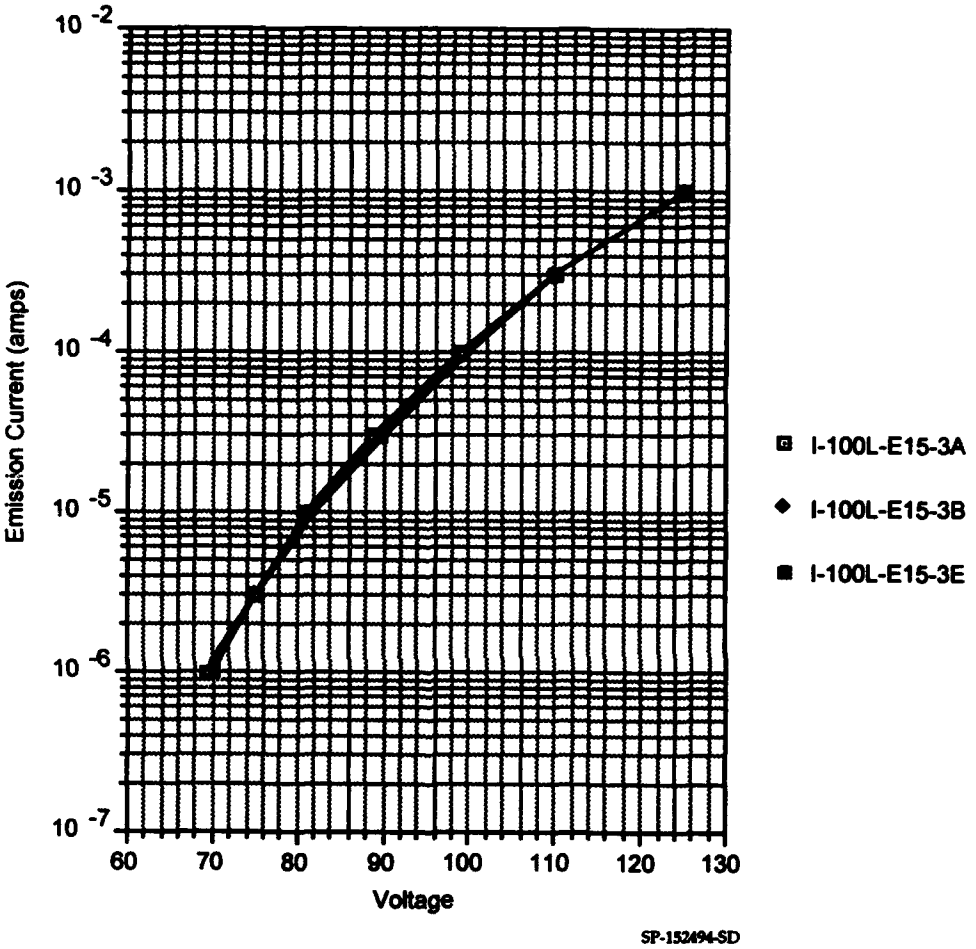

Figure 25. Current/voltage curves for cathodes 100L-E15-3A, B, and E

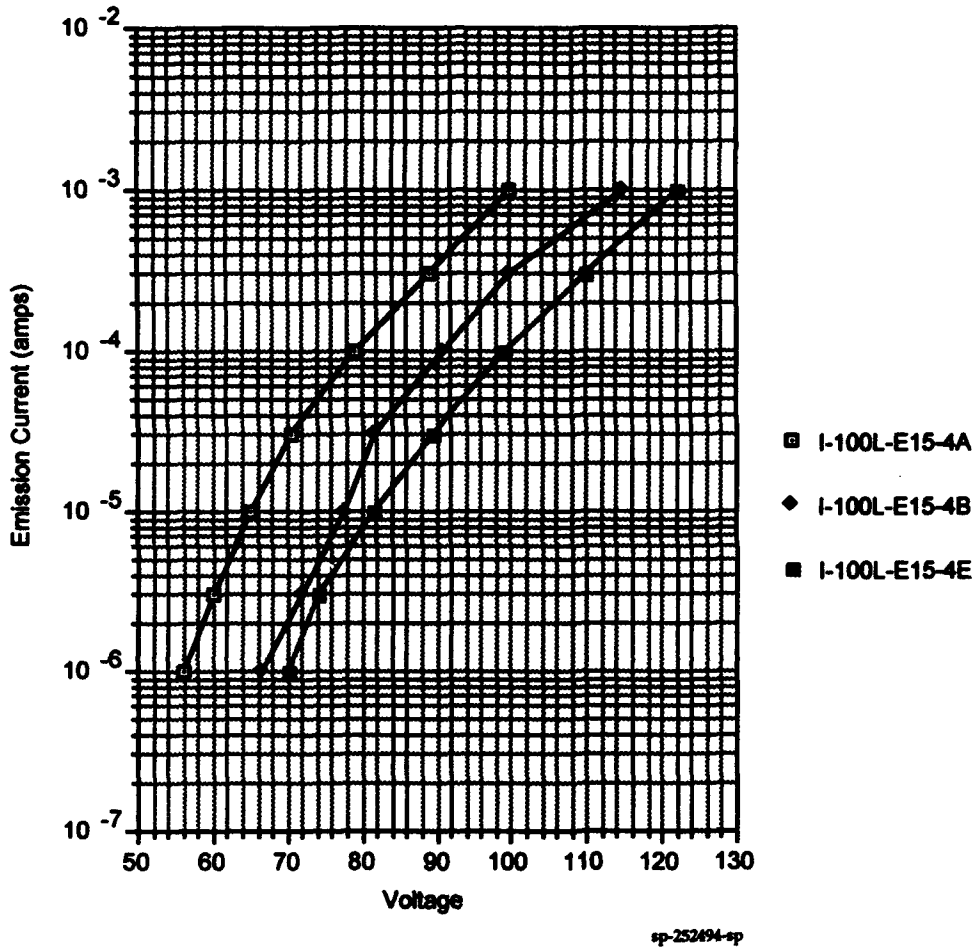

Figure 26. Current/voltage curves for cathodes 100L-E15-4A, B, and E

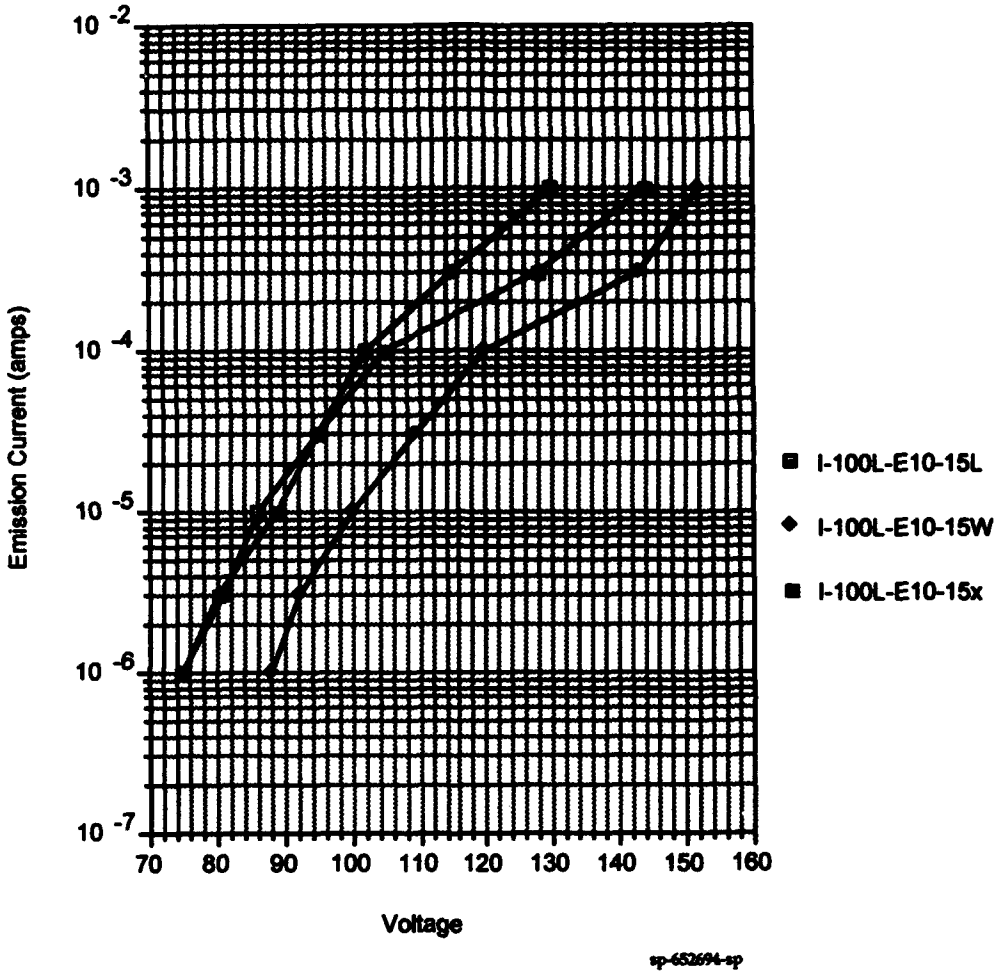

Figure 27. Current/voltage curves for cathodes 100L-E10-15L, W, and X

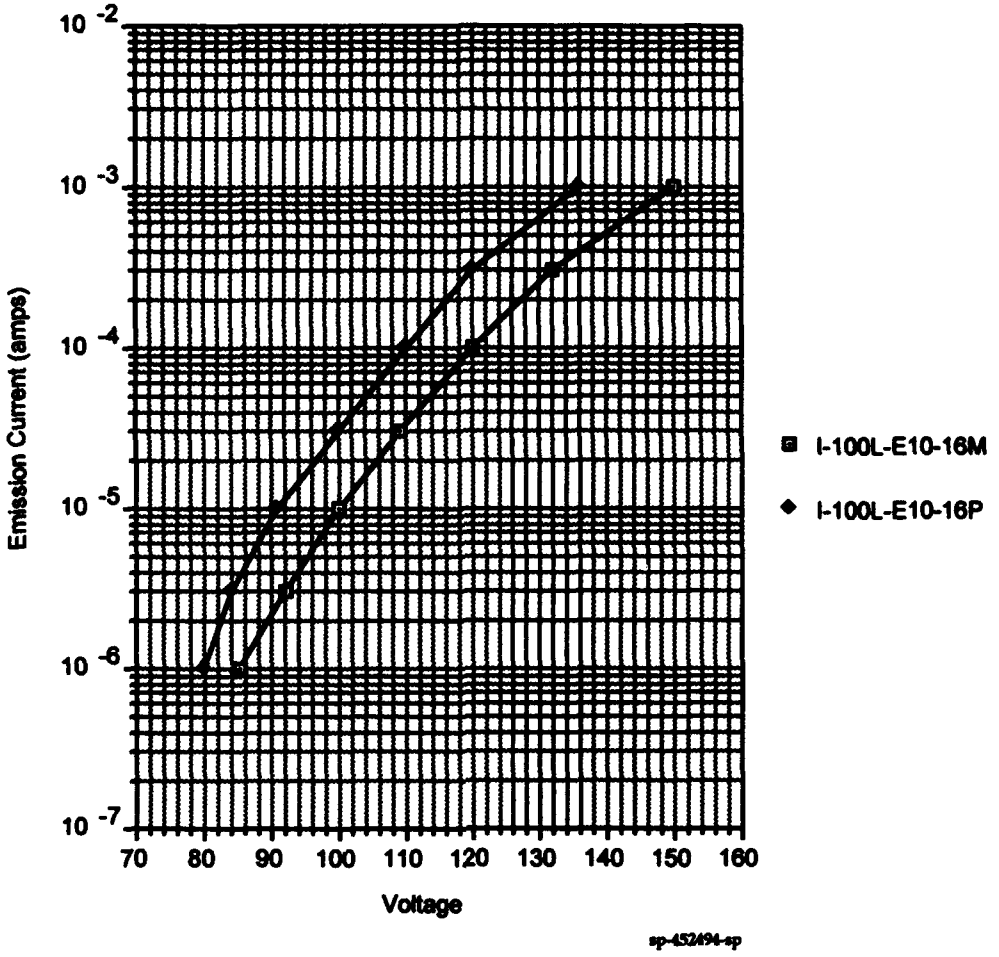

Figure 28. Current/voltage curves for cathodes 100L-E10-16M and P

centers, and others have 625 tips on 2-μm centers. Variations are also due in part to small differences in ß factors (gate aperture diameters and associated tip sharpness) between individual cathodes and the limits of the uniformity it is possible to achieve with the apparatus presently available for fabrication processes.

Untested cathodes from these same four groups were sent to NRL for in-house testing. The cathodes tested at SRI cannot be retested at NRL because it has been impossible to lead bond to the gold contact pads at NRL after the cathodes have been through a test. We assume that chrome diffusing through the gold during bakeout forms an oxide on the surface when it is exposed to air. However, it was agreed that NRL would supply SRI with one of it high-frequency mounts so that SRI could mount, *pretest*, and ship a high-frequency cathode to NRL.

In the meantime, we anticipate improved results at NRL with cathodes that have not suffered from galvanic etching during our final cleanup process.

3.5 TESTS ON HRL STRUCTURES

Emission tests with the submicrometer structures formed in cooperation with HRL have just begun and have been very encouraging. Figure 29 is an oscillograph of the current vs. voltage characteristics for a standard 100-tip array with gate apertures about 1.1 μm in diameter and an HRL patterned 100-tip array, with gate apertures about 0.25 μm in diameter. Both are on our standard silicon substrate. The voltage requirement for the same current with the 0.25-μm–diameter array is less than half of that required for the larger-diameter apertures, and the slope of the current vs. voltage curve is steeper for the smaller cathodes, indicating a higher transconductance as well. The peak emission level is 100 μA, or 1 μA/tip averaged over the array. This was achieved with 44 V applied to the small cathode structure, compared to about 93 V for the larger structure. These are very encouraging first results, and make it clear that the smaller gate aperture fabrication processes are well worth pursuing.

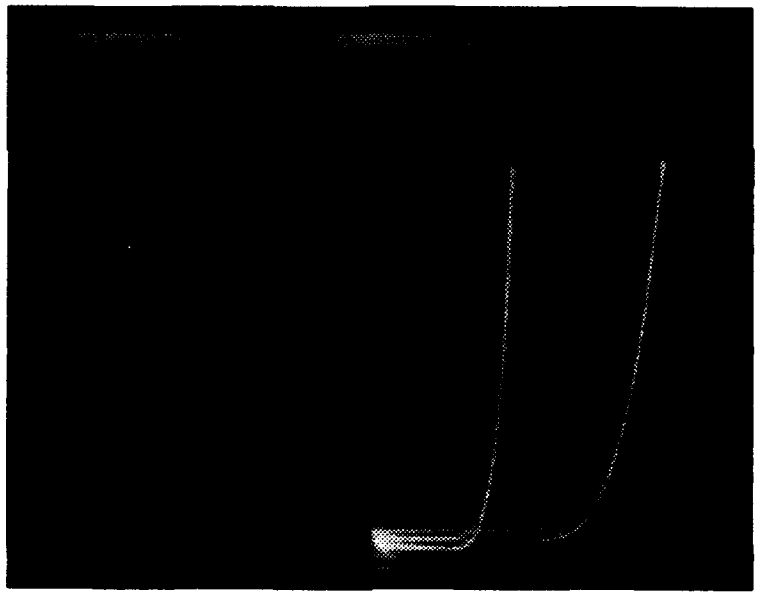

sp-19894-ad

Horizontal: 20 V/major division
Vertical: 20 μA/major division

Figure 29. Current/voltage curves for cathodes FE33B-362-2E (low voltage) and 54i-344-2W (high voltage); the low-voltage cathode has 0.25–μm-diameter gate apertures, and the high-voltage cathode has 1.1-μm-diameter apertures (both are 100-tip arrays)

4. HIGH-FREQUENCY MEASUREMENTS

Using our high-frequency test vehicles, we were able to make measurements with a triode setup at 1-GHz modulation rates early in 1993. Difficulties with the Hewlett-Packard 8510 Network Analyzer prevented us from obtaining satisfactory S parameter measurements at that time. These difficulties appeared to have resulted from the calibration standards that had been prepared for our work.

High-frequency measurements were essentially limited to just demonstrating modulation at 1 GHz because of the complexity of calibrating the system for S parameter measurements.

In June 1993, four cathodes with the electrostatic shield configuration were placed in our high-frequency test apparatus to produce test data for the annual vacuum electronics review. The cathodes were somewhat inferior, because at that time we had not yet completely eliminated the sulfur contamination. Nevertheless, one of the cathodes was carefully nursed into decent behavior. (The other three failed early because of erratic operation, probably resulting from the contamination.)

Measurements of S21 were made at 1, 3, and 5 mA with the *good* cathode. S parameter measurements above 5 mA were not possible because the network analyzer requires that the cathode be ON for at least 1 second for a measurement to be made, and with a 1-second ON time and 20-second OFF time the anode became orange hot at the end of the 1-second ON time. However, enough data were taken to show that the program goal of modulation at 1 GHz had been achieved and that the transmission coefficient (S21) is 3.5 dB greater at 5 mA and 1 GHz than it is at < 1 μA emission. Figure 30 shows the relative magnitudes of S21 for three values of emission.

Figure 31 shows the results of attempts to measure S11 and S22 with the apparatus we have. Clearly something (our calibration standard) is not quite right, because the forward reflection coefficient cannot be greater than 1 (0 dB). We worked with network analyzer specialists in an effort to improve these results, but were unable to produce sufficient improvement within the budget and time constraints of the program.

In the summer of 1993, high-frequency measurements were discontinued so that we could concentrate our remaining resources on fully resolving the contamination issues associated with fabrication processes and further improving the basic cathode structure with regard to transconductance.

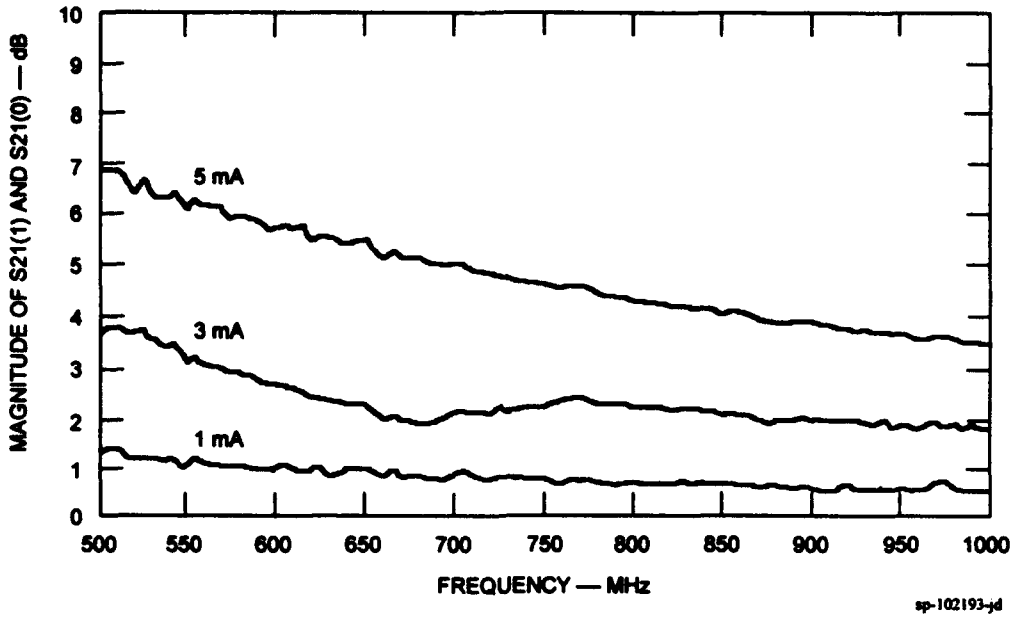

Figure 30. Magnitude of S21 at 1-, 3-, and 5-mA emission levels relative to <1 μA emission for cathode 102L-E10+5C

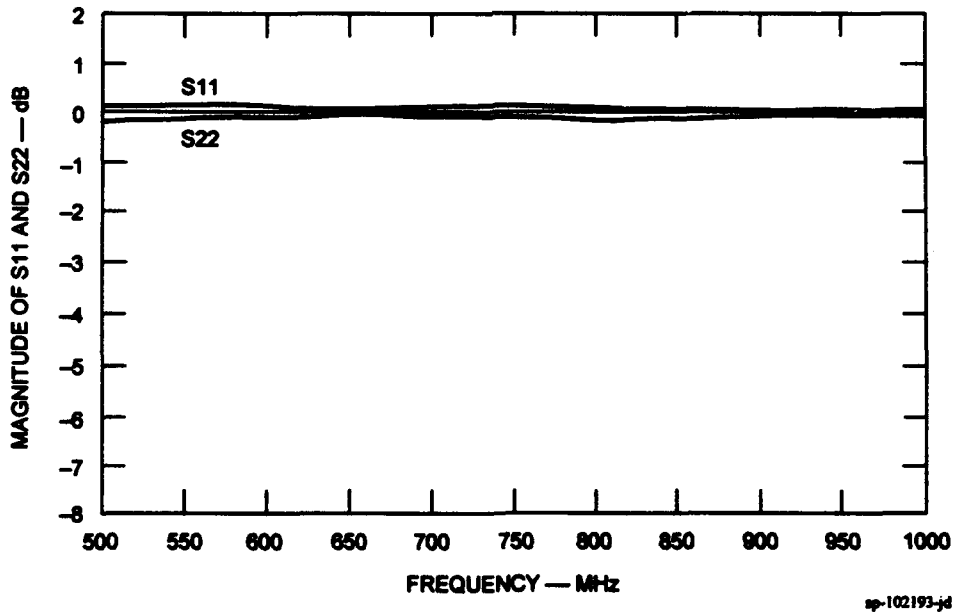

Figure 31. Measured forward and reverse reflection coefficients for cathode 102L-E10+5C showing an obvious error in the S11 parameter, probably due to an imperfect calibration standard

5. PROCESSING TO IMPROVE PERFORMANCE, YIELD, AND RELIABILITY

Late in the project, work continued on our study of the emitter array's performance and its improvement. We have conducted Müller microscope imaging, Auger spectroscopy, and observations of the effects of plasma treatments and various gas environments with the aid of the Müller microscope. We also worked on assembling and activating an emission microscope obtained on loan from Hughes Aircraft. The instrument is elegantly simple in principle, but does require some learning and alignment to achieve a useful image. The objective is to image an array with sufficient magnification and resolution of each individual tip that we can determine uniformity of emission from tip to tip over the array, as well as the effects of various treatments on the uniformity of emission. By early March 1994, the microscope was ready for its first trial.

We continued to study the effects of processing on cathode performance. Specifically, hydrogen plasma cleaning was fruitful. A Müller-type emission microscope apparatus was fabricated for studies of cathode processing. The system is capable of operating a cathode at temperatures as high as 900 K, or at liquid nitrogen temperature, and has a provision for plasma-treating the surfaces and deposition of material onto the cathodes *in situ*.

5.1 MÜLLER MICROSCOPE STUDIES OF CLEANING PROCESSES

The first experiments with cathode processing involved plasma cleaning with hydrogen. A cathode was mounted in the system, baked at 250 °C overnight, and tested to produce Fowler/Nordheim data at a base pressure of 5×10^{-11} torr. The cathode was then exposed to a dose of $\sim 1 \times 10^{18}$ hydrogen ions/cm^2 from a 300-V, 5×10^{-1} torr plasma in 2.5 minutes. The emitter tips and gate film were connected and formed the cathode in the dc plasma. The anode was approximately 1 cm from the cathode.

After the plasma treatment, the hydrogen was pumped out of the system, and the cathode was again operated to gather Fowler/Nordheim data. The results of measurements made before and after the treatment are shown in Figure 32. Examination of the data shows that an increase in emission current of between one and two orders of magnitude was achieved with an apparent decrease in work function of 1.1 eV as the result of the hydrogen plasma cleaning. In addition, observations of the emission patterns on a phosphor screen showed qualitative improvements in the emission uniformity from the array as the result of the treatment. However, the resolution of the apparatus was not sufficient to obtain quantitative data on uniformity.

The emission was stable after the plasma treatment, and unchanged after 100 hours of operation in a vacuum of $\sim 3 \times 10^{-11}$ torr. This was interesting in light of earlier work showing that the emission drifted back to some value between the values before and after plasma treatment when the base pressure was $\approx 3 \times 10^{-9}$ torr. This was further evidence that the emitter arrays tend to come to equilibrium with their operating environment, and once the surfaces are cleaned the environment plays an important role in performance.

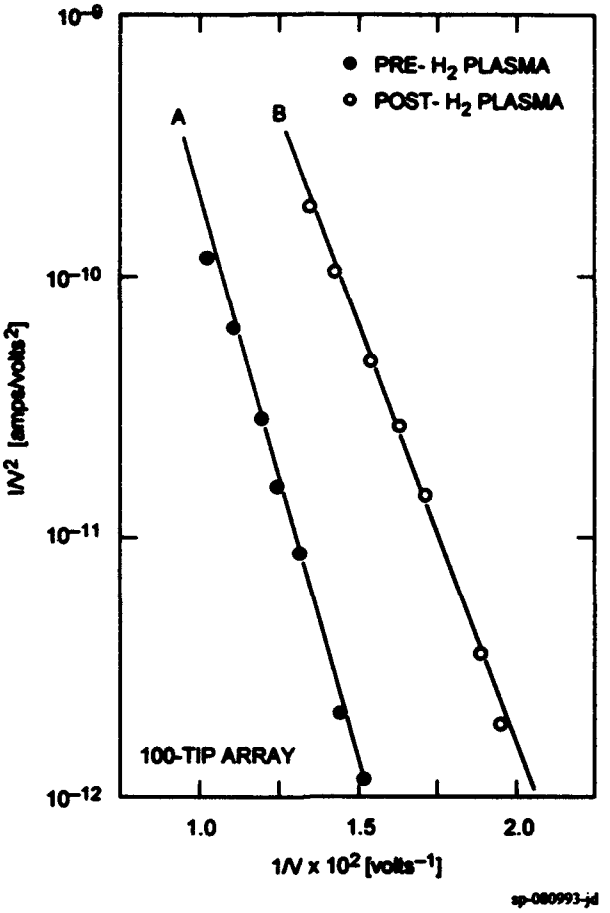

Figure 32. The effect of hydrogen plasma treatment on a 100-tip array. Line A: Fowler-Nordheim data prior to hydrogen plasma treatment. Line B: Fowler-Nordheim data following hydrogen plasma treatment (dose ~ 10^{18} ions/cm^2). The apparent work function decrease is 1.1 eV.

Results of our work on plasma cleaning processes were submitted for publication to the *Journal of Applied Physics*. A preprint of the paper is attached as an appendix.

5.2 EMISSION MICROSCOPE WORK

Significant effort was directed toward activating an emission microscope obtained on loan from Hughes Aircraft in Torrance, California, early in 1994. The instrument is elegantly simple in principle, but requires some learning and alignment to achieve a useful image. The objective is to image an array with sufficient magnification and resolution to resolve each individual tip and determine uniformity of emission from tip to tip over the array, as well as the effects of various treatments on the uniformity of emission over the array. We achieved an image of a 1000-tip array, but some fine tuning is required to resolve individual tips clearly. Figure 33 is a photograph of the image of a 1000-tip array taken during the early stages of emission. The total emission current is only 10 μA. Clearly, not all of the emitter tips are contributing. However, the early observations have been that as the emission is increased, more

Figure 33 An image of the emission pattern from a 32 x 32 array of emitter tips; the total emission current is 10 μA, and phosphor voltage is 1200 V

and more tips become active, and that the overall uniformity also tends to improve with time. This suggests that a burn-in or conditioning period will be beneficial. However, as a practical matter, the time required for burn-in is excessive (sometimes days), and a fast surface processing procedure such as plasma cleaning is needed to replace the burn-in.

The next steps would be to improve the resolution and begin experiments with surface treatments to accomplish improved uniformity of emission over the entire surface of the array from the onset of emission.

5.3 MÜLLER MICROSCOPE STUDIES OF EMITTER-TIP COATINGS

Additional studies to enhance field-emitter array performance using our Müller microscope focused on the vacuum deposition of coatings following array fabrication. Of several elemental coatings investigated, titanium has shown very promising results.

Titanium coatings have been shown to lead to increases in current at a given voltage by a factor of ~10^2 to 10^3 when compared to the cathode prior to coating. In addition, the emission stability of the cathode increases by greater than a factor of 10.

Late in the project, experiments were conducted in order to quantify this relatively dramatic improvement in the cathode's operational characteristics. Collected data are suggestive of a preliminary explanation.

Standard analysis of the cathode's current/voltage (I/V) characteristics yields information regarding the cathode's average work function Φ, electric field-voltage proportionality factor β ($E = \beta V$), and emitting area A, through the Fowler-Nordheim (FN) equation[1]

$$\ln (I/V^2) = \ln aA + b/V \quad (1)$$

Here I is the electron current and

$$b \propto \Phi^{3/2}/\beta \quad (2)$$

and

$$a \propto \beta^2/\Phi \quad (3)$$

Plotting the cathode's current/voltage characteristics in the form of Eq. 1 [$\ln(i/V^2)$ vs I/V^2] yields a straight line having an $\ln(I/V^2)$ intercept proportional to the emitting area and a slope proportional to $\Phi^{3/2}/\beta$.

Analysis of our data shows that titanium deposits lead to an increase in emitting area by a factor of $\approx 10^2$ to 10^3 and very small initial changes in slope. As the electron current is proportional to the emitting area (see Eq. 1) the increase in current of 10^2 to 10^3 observed following titanium deposition is explained. In addition, the fluctuations in the electron current can be shown[2] to vary as $\sqrt{A}$, meaning that the emission fluctuations should be reduced by 10 to 30 times after the deposition of titanium, also in agreement with the experimental results.

The question remains, however, why does the emitting area increase following the deposition of titanium?

It is generally accepted that the emission from as-fabricated emitter-array tips emanates from only a few atomic sites.[3] This implies that the increase in emitting area due to the addition of titanium is the result of a smoothing of the emitter-tip surface—that is, titanium fills in the area between the emitting (protruding) atoms, creating a more atomically smooth surface from which electron emission occurs more uniformly. This would also lead to a decrease in β by a factor of ≈ 3, assuming a protruding atom has a field enhancement factor of 3—that is, that of a hemisphere on a plane.[4] Then the slope of the FN plot should be increased approximately three times due to its dependence on β, a result that is not observed. We can explain this apparent discrepancy if we recall[5] that the deposition of zirconium and hafnium on molybdenum and tungsten surfaces results in a work function decrease of ≈ 2 eV due to the electropositive nature of zirconium and hafnium. As titanium has nearly the same electropositive characteristic as zirconium and hafnium, we would expect a roughly similar result when titanium is deposited on molybdenum. Referring to Eq. 2,

$$b_{Ti}/B_O = (\Phi_{Ti}/\Phi_O)^{3/2} \{\beta_O/\beta_{Ti}\} = (2.3 \text{ eV}/4.3 \text{ eV})^{3/2} \{\beta_O/[\beta_O/3]\} \approx 1.2$$

where b_O and b_{Ti} are the slopes in Eq. 1 prior to and following titanium deposition, respectively. This relatively small change in slope is consistent with experimental observations. Thus, the reduced work function due to titanium deposition is apparently offset by a decrease in β due to smoothing of the emitter surfaces. The significant reduction in voltage for a given current and the decrease in emission current fluctuations can be thought of as being primarily associated with an increased effective emitting area.

This situation is nearly ideal as the operational voltage is reduced and the current stability is simultaneously increased, the decrease in β being offset by a decrease in Φ.

6. SUMMARY OF PROGRAM ACCOMPLISHMENTS

All program goals have been met or exceeded. The principal goals were 5 mA at 5 A/cm^2 and modulation at 1 GHz. Emission currents of up to 25 mA and 1000 A/cm^2 were achieved, as was emission modulation at 1.3 GHz. In addition, eventual modulation at tens of GHz was shown to be feasible because of improvements in emitter-tip packing density and transconductance per tip that have resulted from advanced lithography techniques along with improved cone deposition processes that have increased the emitter cone aspect ratio (height-to-base-diameter ratio). These improvements make it feasible to increase the transconductance significantly without causing an equivalent increase in device capacitance.

REFERENCES

1. R. Gomer, *Field Emission and Field Ionization*, Harvard University Press, Cambridge, MA, 1961.
2. H.D. Beckey, *Field Ionization Mass Spectrometry*, Pergamon, New York, 1971.
3. C.A. Spindt, et al., *J. Appl. Phys.* **47**, 5248, 1976.
4. J.A. Stratton, *Electromagnetic Theory*, McGraw Hill, New York, 1941.
5. L.W. Swanson and N.A. Martin, *J. Appl. Phys.* **46**, 2029, 1975.

Appendix A

PUBLICATIONS AND PRESENTATIONS SUPPORTED BY ARPA CONTRACT MDA972-91-C-0029

Results and progress of the research program supported by ARPA under Contract MDA972-91 C-0029 were reported by SRI scientists in the following publications and presentations:

C. Holland and C. Spindt, "Field-Emission-Array Development for High-Frequency Operation," Tri-Service/NASA, March 1994.

C. Spindt, C. Holland, A. Rosengreen, and I. Brodie, "Field-Emitter-Array Development for Gigahertz Operation," IEDM/IEEE, July 1992.

C. Holland and C. Spindt, "Field-Emitter-Array Development for High-Frequency Operation," *J. Vacuum Science Technol.*, March/April 1993.

P. Schwoebel, "Recovery of Luminous Efficiency of Degraded Willemite Phosphor in an Oxygen Glow Discharge," *J. Electrochem Soc.*, March 1993.

P. Schwoebel and C. Spindt, "Field-Emitter-Array Performance Enhancement Using Hydrogen Glow Discharge," *J. Appl. Phys. Lett.*, January 1993.

P. Schwoebel, I. Brodie, and C. Spindt, "Field-Emitter-Array Performance Enhancement Using Hydrogen Glow Discharge Processing," *J. Appl. Phys. Lett.*, March 1993

C. Spindt, C. Holland, A. Rosengreen, and I. Brodie, "Progress in Field-Emitter Development for Gigahertz Operation," IVMC Conference, March 1993; 40th Int'l Field Emission Symp., June 1993.

C. Spindt, C. Holland, A. Rosengreen, and I. Brodie, "Field-Emitter-Array Development for High-Frequency Operation," *Vacuum Electronics Committee Rev.*, June 1993.

C. Holland, A. Rosengreen, I. Brodie, and C. Spindt, "Progress in Field-Emitter-Array Development for High-Frequency Operation, *IVMC Proc, AIP*, October 1993.

P. Schwoebel and C. Spindt, "Glow Discharge Processing to Enhance Field-Emitter-Array Performance," *J. Appl. Phys.*, 24 September 1993.

C. Spindt and C. Holland, "Microstrip-Line Integrated Field-Emission Cathode for High-Frequency Operation," Microwave Power Tube Conference, January 1993.

P. Schwoebel, C. Spindt, I. Brodie, and C. Holland, "In-Situ Enhancement of Field-Emitter Array Performance," 7th Int'l Vacuum Microelectronics Symp. (IUVSTA), July 1994.

C. Spindt, C. Holland, I. Brodie, and P. Schwoebel, "The Fabrication and Performance of Gated Field-Emitter Arrays with Nanometer Feature Sizes," 7th Int'l Vacuum Microelectronics Symp. (IUVSTA), July 1994.

I. Brodie, "Modifications to the Fowler-Nordheim Theory to Account for Surface-Structure and Conduction Electron Energy Distribution," 7th Int'l Vacuum Microelectronics Symp. (IUVSTA), July 1994.

Appendix B

GLOW DISCHARGE PROCESSING TO ENHANCE FIELD-EMITTER-ARRAY PERFORMANCE

Glow discharge processing to enhance field-emitter array performance

P.R. Schwoebel [Telephone: (415) 859-4845, FAX: (415) 859-3090] and

C.A. Spindt [Telephone: (415) 859-2993, FAX: (415) 859-3090]

SRI International, Menlo Park, California 94025

(Received

ABSTRACT

Changes in the electron-emission spatial distribution and I-V characteristics of microfabricated field emitters following inert gas ion bombardment have been investigated. The combination of glow discharge treatments in hydrogen and neon result in contaminant removal and mild emitter tip sputtering, thereby leading to significant improvements in the uniformity of the electron emission from individual tips and between tips in the arrays. The majority of the enhancement in the uniformity of the electron emission appears to be due to a net smoothing of the emitter tip surfaces through the removal of field-enhancing protuberances by the inert gas ion bombardment.

PACS numbers: 79.70.+q, 79.20.Nc, 81.60.Bn

I. INTRODUCTION

Microfabricated field-emitter arrays are presently being investigated for use in such technologically important applications as microwave amplifiers and flat-panel displays.[1] To facilitate their incorporation into various devices, we are investigating processing procedures through which the performance of field-emitter arrays can be enhanced.

This performance enhancement is a multifaceted goal involving such aspects as operational voltage reduction, the rapid achievement of emission current stability at relatively high current-per-tip loading levels ($I > 10\ \mu A$/tip), and increasing emission current uniformity from each tip and between tips in the array. To quantify the basic principles involved in array performance enhancement, we recall the Fowler-Nordheim equation,[2,3] which describes the current-voltage (I-V) characteristic of the electron field-emission process,

$$I/V^2 = \alpha a\, \beta^2 \exp(-b\phi^{3/2}/\beta V).$$

Here, I is the electron current, V the applied voltage, *a* and *b* are essentially constants, α is the emitting area, ϕ is the average work function of the emitter surface, and β is the proportionality factor between the applied voltage and the electric field, E, at the emitting surface, $E = \beta V$.

It is clear that to enhance emitter array performance one must control ϕ and β; that is ϕ and β should optimally be identical from tip to tip in the array. This amounts to controlling the chemical state and physical structure of the emitter array surfaces. Therefore, any post array fabrication processing procedures developed to enhance performance are best performed *in situ* prior to, or following, tube seal-off.

The first step towards control of the emitter surface chemistry is to "clean" the emitter array surfaces. During their fabrication and handling, exposure to the ambient atmosphere will lead to carbonaceous surface contamination and in many cases oxidation.[4] Previous investigations have shown that *in situ* hydrogen plasma treatment to ion doses of 10^{18} to 10^{19} ions/cm^2 results in a work function decrease of ~ 1 eV and improvements in the emission uniformity in the case of both microfabricated single tips and arrays.[5] This is presumably due to the removal of the surface contaminants. The cleaning action of the hydrogen reaches completion as there exists a dose in the range of 10^{18} to 10^{19} ions/cm^2 beyond which no further changes in the I-V characteristics are observed. Lastly, preliminary investigations have shown that contaminant removal via hydrogen plasma treatment allows for *immediate* turn-on of the array to relatively high current-per-tip loading levels (≥ 5 μA/tip) without disruptive vacuum arcs that lead to emitter tip array destruction. In the past, array destruction could occur frequently if relatively long emitter seasoning procedures were not employed wherein gradual increases in emission current were made until the final operating level was reached; seasoning time periods could be on the order of 50 to 100 hours.

Given the apparent surface cleanliness achieved with hydrogen glow discharge processing we turn to the question of further enhancing emission uniformity across emitter arrays; this to a large degree focuses on the detailed geometrical structure of the emitter tips at their apices.

Control of the geometrical structure of the emitter array surfaces can be considered on two approximate length scales L_1 and L_2, where $L_1 \geq 100$ Å and $L_2 < 100$ Å. The L_1 range is fairly well controlled in modern microfabrication processes; in the case of emitter arrays this refers to the general tip shape, gate hole diameters, tip-to-gate spacing, and so forth. In the range of L_2, however, many factors emerge, particularly involving details of the emitter tip shape, which are difficult to control and have a profound effect on β. For example, in the case of polycrystalline emitter tips grain size, shape, and orientation are important. In addition, for all

types of emitter tips the presence of clusters of surface atoms and the resulting field-enhancing effects should be expected. For reference we recall that a conducting hemisphere on a conducting flat plane produces a field enhancement factor of 3 at its apex over that of the field on the plane far removed from the hemisphere.[6] As the emission current is exponentially dependent on β, the details of the emitter tip shape at length scales of < 100 Å are very important and some degree of control over these physical aspects is required if emission uniformity across the array is to be achieved.

In the research presented here we have studied the effects of combining hydrogen plasma treatment with glow discharges involving inert gases to investigate the effect on ϕ and β of supplementing the chemical cleaning action of the hydrogen with the sputtering action of relatively low energy inert gas ions. Relatively high energy inert gas ion bombardment (> 1 keV) is commonly employed for the sputter cleaning of surfaces[4] and the sharpening of conventional field-emitter tips.[7]

II. EXPERIMENTAL

The experimental chamber is an ultra-high vacuum (UHV) field-emission microscope constructed of metal and glass with a base pressure of $< 3 \times 10^{-11}$ torr following a 12-hour bakeout at 250 °C. All experiments were conducted at room temperature.

Array performance data is collected in the form of I-V characteristics and by direct viewing of the electron-emission spatial distribution on a phosphor screen.

The microfabricated emitter tips were of the type developed at SRI: metal-insulator-metal, employing SiO_2 as the insulating layer between a molybdenum gate and molybdenum emitter tips, as shown in Figure 1.

Glow discharges were operated with a current-regulated direct current supply. During glow discharge processing the base and gate of the emitter array were electrically connected and served as the cathode in the discharge; thus, the array structure was bombarded only by ions. The anode of the glow discharge was ~1 cm from the cathode. At this distance, pressures of ~1 torr and operating voltages of ~275 to 450 V were required to sustain a glow discharge in the gases employed. Total ion current densities at the emitter array were on the order of 1×10^{16} ions/cm^2/s. Gases used were research-grade purity (99.9999%) and admitted to the system from 1-*l* glass flasks. Following glow discharge treatment the system was evacuated to UHV conditions prior to array operation.

III. RESULTS

To determine the effects of inert gas ion bombardment on emitter array performance, the arrays were first cleaned by hydrogen plasma treatment. This procedure was used to produce chemically similar surfaces with which the changes produced by subsequent bombardment with various inert gas ions could be investigated.

A. Hydrogen and neon glow discharges

Following installation of the emitter array in the microscope and system bakeout, I-V characteristics were collected from the emitter array. An example of such data, for a 127-tip array, is shown in Figure 2 (curve A) as a Fowler-Nordheim (FN) plot.

Next, the array was treated in a hydrogen glow discharge under the conditions described above to a dose of 10^{18} ions/cm^2. The initial results of hydrogen glow discharge cleaning of emitter arrays have been reported.[5] After evacuating the system to UHV conditions the I-V data shown in curve B of Figure 2 were accumulated. Note the reduction in voltage required to

achieve a given current relative to the I-V characteristics shown in curve A. The field-emission micrographs corresponding to the FN data in Figure 2, curves A and B, are shown in Figures 3a and 3b, respectively. Note in the patterns that although the change in the emitting area appears to be rather small there is an increase in the emission uniformity. This was typically observed with all emitter arrays studied.

To investigate the effects of mild sputtering on array performance, hydrogen cleaning was followed by neon bombardment. The results of glow discharge processing using He + 10% Ne and H_2 + 10% Ne to equivalent ion doses were similar. Curve C, Figure 2, shows the I-V characteristics of the 127-tip array following treatment in H_2 + 10% Ne to a total ion dose of 2×10^{19} ions/cm^2 (~2×10^{18} ions/cm^2 of Ne^+). In general, the slope following H_2 + 10% Ne treatment varied from being slightly less than to slightly greater than (but within ~10% of) the slope of the post-H_2 treated array. However, a sufficient ion dose could be achieved after which: (1) the slope of the post-H_2/Ne-plasma-treated array FN data was approximately equal to or greater than for the hydrogen-plasma-treated array (curve B), and (2) a decrease in emission current at a given voltage relative to curve B occurred.

The effect of this treatment as observed in the electron-emission pattern, shown in Figure 3c, is very interesting. We note that our 127-tip arrays are fabricated such that the border of the array is a hexagon. This hexagonal shape is evident in the emission pattern of Figure 3c; for reference, the orientation of the hexagon is shown in the upper right corner of the figure. The appearance of the array shape in the emission pattern following Ne/H_2 plasma treatment was often observed with the 127-tip arrays and the 100-tip arrays (square pattern due to the 10 × 10 packing arrangement) that we have investigated. These observations indicate that such treatment significantly enhances emission uniformity across the arrays; we estimate that *at least* 50% of the tips in the array must be participating in the emission process for such a definition of the array shape to result.

Ne/H_2 treatment induces changes in the I-V characteristics and emission pattern up to Ne^+ doses of typically ~ 10^{18} ions/cm^2; thereafter, changes are much slower following an equivalent dose.

Similar experiments have also been conducted employing single microfabricated field-emitter tips. In general, the changes in the I-V characteristics of the single emitter tips were similar to those observed with the arrays. However, in particular cases the emission current at a given voltage could be increased at some point with H_2/Ne bombardment as is discussed below.

The FN data are shown in Figure 4 for a single tip. Curve A is the data following installation in the system and bakeout. After hydrogen plasma treatment to a dose of 10^{18} ions/cm^2, the data in curve B were collected. Again, note the reduction in the voltage required for a given current when compared with curve A. The field-emission patterns corresponding to the pre- and post-hydrogen-plasma-treated tip are shown in Figures 5a and 5b, respectively. A slight increase in the emitting area is observed and a distinct improvement in the emission uniformity has occurred. This was a general trend observed with single emitter tips. Note that in the case shown here, hydrogen plasma treatment resulted in the disappearance of a spurious emission site in the lower right corner of the pattern in Figure 5a. This indicates that the large emitting area shown in Figures 5a and 5b is a region that protrudes from the emitter tip apex.

Following the hydrogen plasma treatment the emitter was exposed to the H_2 + 10% Ne plasma. Curve C shows the I-V characteristics after a dose of ~1×10^{17} ions/cm^2 of Ne, and curve D after ~ 7×10^{17} ions/cm^2 Ne. Note that in curve C the current for a given voltage has increased relative to curve B. However, following a sufficient Ne dose the emission current for a given voltage decreases relative to curve B, as shown in curve D. The field-emission pattern corresponding to curve D is shown in Figure 5c. A significant increase in emitting area and emission uniformity is evident in the micrograph.

B. Hydrogen and xenon glow discharges

The experiments involving Xe and H_2 were conducted in the same manner as those involving Ne and H_2. Again, the results for arrays and single emitter tips were similar.

Following installation of a single tip and system bakeout, the I-V characteristics shown in curve A, Figure 6, were collected. Hydrogen plasma treatment to a dose of ~ 1×10^{18} ions/cm^2 resulted in the subsequent I-V characteristic shown in curve B of Figure 6. The corresponding field-emission patterns for the pre- and post-hydrogen-plasma-treated emitter are shown in Figures 7a and 7b, respectively. Note again that the decrease in voltage for a given current is accompanied by an increase in the emission uniformity from the emitter tip.

Plasma treatments involving H_2 + 10% Xe were subsequently performed. Curve C in Figure 6 shows the I-V characteristics obtained after a dose of 5×10^{16} ions/cm^2. Figure 7c is a field-emission micrograph of the emitter taken following the I-V characteristics of curve C, Figure 6. H_2/Xe treatment often resulted in the currents for a given voltage exceeding those required prior to hydrogen plasma treatment for single emitter tips and arrays. Following a subsequent dose of ~ 5×10^{17} ions/cm^2 the emitter tip was shorted (gate to base). As opposed to Ne (and He) treatments, the occurrence of emitter destruction and/or the presence of gate to base leakage was higher when arrays and single tips were exposed to the H_2/Xe discharge, even at a lower total ion dose.

C. Hydrogen and helium glow discharges

The effects of helium ion bombardment on emitter array characteristics were also investigated under conditions similar to those utilized for neon and xenon. With mixtures of H_2 + 10 % He, applied potentials of ~300 V, and doses of ~10^{18} ions/cm^2, only small changes in the I-V characteristics of the post-hydrogen-plasma-treated arrays and single tips were observed. Voltages for a given current increased by a few percent and small increases in slope (<10 %)

occurred. In addition, only slight changes in the emission patterns were observed with a barely perceptible increase in emission uniformity.

IV. DISCUSSION

To analyze our results, we begin by estimating the ion energies at the cathode (array) under our glow discharge conditions. The ion energies in a relatively high pressure glow discharge, as is the case here, are distributed from near zero to the full anode-to-cathode potential, V_0, making detailed characterization difficult. A reasonable estimate of the "average" ion energy can be found if we calculate the energy of ion type x, E_x, gathered in a mean free path, λ, in the cathode dark space.[8,9]

$$E_x = [\sqrt{2}\,\lambda_x]\, V_{0x}/d_x.$$

where d_x is the thickness of the dark space for the discharge involving ion x. We assume that the entire applied voltage appears across the cathode dark space, thereby maximizing the energy. The $\sqrt{2}$ term corrects for the ionic as opposed to the neutral molecular mean free path.[10]

With d ~ 0.1 cm in all cases, the applied potentials and calculated ion energies are shown in Table 1. The λ's shown in the table are calculated for the gas mixtures shown and apply to the inert gas ion component.[10] We see that these ion energies are well below the sputtering threshold energies of molybdenum—that is, the majority of ions do not sputter the emitter tips. To obtain an absolute maximum on the sputtering yield, Y_{max}, we can take the ion energy to be the full anode-to-cathode potential V_0. This upper limit to the sputtering yield can be found from a combination of experimental data and empirical formulae[11,12]; these yields, for an ion dose, D, are also shown in Table 1. It should be noted that significant errors in the sputtering yield can result from relatively small errors in the ion energy calculation as the sputtering yields are not

well known and in addition are a sensitive function of energy for energies of ~ 100 eV, particularly in the cases of Ne and Xe.[12]

A. Hydrogen

In the case of the pure hydrogen plasma, as has been discussed,[5] it is reasonable to assume that a work function change due to contaminant removal accounts for the shift in the I-V characteristics as the sputtering of molybdenum by hydrogen at the energies and doses investigated here is totally negligible; even at doses of 10^{19} ions/cm^2 H_2^+ with the full cathode-to-anode potential energy of 300 V and neglecting the dissociation of the molecular ion upon impact, only ~10^{-1} monolayers of molybdenum would be removed. The work function change can be extracted from the slope of the FN curves shown in Figure 2.[3,5] If we assume that the average work function of the emitters following hydrogen plasma treatment is that of hydrogen-covered molybdenum, 4.9 eV, we find that hydrogen plasma treatment reduced the effective work function of the array (Figures 2 and 3) by 1.5 eV, and the single tips by 1.4 eV (Figures 4 and 5) and 0.5 eV (Figures 6 and 7). Typical work function changes are 1 eV for hydrogen ion doses of 10^{18} to 10^{19} ions/cm^2; however, changes ranging from 0.5 - 1.5 eV with single tips and arrays have been observed.[5] The resulting slight increases in emitting area and uniformity of the arrays following hydrogen treatment are due to the participation of more tips in the emission process and an improvement in the uniformity of emission from those tips participating.[5]

B. Helium

In helium bombardment, the average ion energies calculated are again near or below the threshold energy for sputtering of the molybdenum tips. The upper limit to the yield, as shown in Table 1, is ~ 2 monolayers of molybdenum for the doses investigated here. The slight changes in the I-V characteristics and emission patterns observed are most likely due primarily to atom displacements by ion-bombardment-activated surface diffusion. This hypothesis is consistent with the fact that the slight changes in the I-V characteristics rapidly saturate; that is for doses of

~ 10^{16} ions/cm^2 to ~ 10^{17} ions/cm^2 of helium no significant changes in the I-V characteristics occur, and only slight variations in the details of the emission pattern are observed.

C. Neon and xenon

The situation in which surface sputtering is nonnegligible is rather complicated to explain unequivocally. It is clear from the emission patterns of single tips and arrays that the emission area and uniformity are significantly increased following H_2/Ne and H_2/Xe plasma treatment. Such an improvement has not been observed with H_2 treatment alone. Unfortunately, the physical details leading to the changes observed in I-V characteristics are difficult to extract from the FN data. We have, of course, three variables—the area α (proportional to the intercept of the FN plots), ϕ, and β. Although ideally emitting areas can be found directly from the FN data without a detailed knowledge of ϕ or β, the presence of surface adsorbates can severely skew these calculations. In our case, large amounts of chemisorbed hydrogen are most likely present on the emitter surfaces. As hydrogen is known to decrease the microscopic emitting area of tungsten emitters[13] by a factor of ~10, we would expect to see such a result with molybdenum as the two are chemically similar. This unknown variation in α, in addition to the fact that the FN intercept depends on ϕ and β, makes changes in the FN intercepts difficult to interpret. A qualitative explanation of the changes in the slope of the FN plots induced by inert gas ion bombardment is possible, however.

Inert gas ion bombardment is observed to lead to an increase in slope of the FN plots. We recall that the slope of the FN plot, S_{FN}, varies as

$$S_{FN} \propto \phi^{3/2}/\beta.$$

During the initial stages of inert gas ion bombardment, we might expect to see changes in both ϕ and β. Some initial atomic-scale surface roughening should occur, and can be accounted for by an effective *decrease* in the average surface work function. This follows from the fact that low-index (atomically smooth) crystal planes have a higher work function than high-index

(atomically rough) crystal planes.[14] The average surface work function may also be decreased by the sputtering of contaminants not removed by the hydrogen plasma treatment. Both of these factors in themselves would lead to a decrease in the slope of the FN plot, a trend that is not observed. Thus, we conclude that decreases in β dominate the change (increase) in slope observed following bombardment. The changes in the I-V characteristics observed with Ne and Xe are generally consistent with this hypothesis. The sputtering and ion-bombardment-activated surface diffusion apparently lead to a net smoothing of the emitter surface and therefore a decrease in β. Note that as protuberances present a greater surface-area-to-volume ratio than does the bulk structure of the emitter tip, their preferential sputtering and/or dispersion would be expected. The subsequent increase in emission uniformity is due to the variation in sputtering rate with the emitter tips' β. The β of 'blunt' tips changes more slowly because of sputtering than does the β of relatively 'sharp' emitter tips—that is, more material must be removed from a large tip, relative to that required for a smaller tip, to achieve an equivalent change in β. Thus, the emitter tips tend to approach an equilibrium shape, thereby leading to an enhancement in emission uniformity across the array.

Because of the large ion energy spread in the glow discharge, it is difficult to quantify the quantity of emitter tip material sputtered during our investigations. From our ion energy calculations we can conclude only that for inert gas ion doses of 10^{18} ions/cm^2, much less than ~ 30 and 70 monolayers of molybdenum are removed by Ne^+ and Xe^+, respectively. Although the calculations indicate that the absolute yield of molybdenum for a given ion dose is of the same order for Ne^+ and Xe^+, we observe relatively dramatic changes in the I-V characteristics for Xe^+ doses only on the order of 10^{16} to 10^{17} ions/cm^2. In addition, the use of Xe, despite the improvement in uniformity observed, often leads to leakage (base to gate) and/or apparent vacuum-arc-intitiated emitter tip destruction. Neon bombardment reproducibly leads to significant improvements in emission uniformity without causing leakage and arcing as is often the case with Xe. At this point, we have been unable to reconcile this discrepancy. If it were

possible to calculate or measure the ion energy distributions, and thereby determine accurate sputtering yields for Ne and Xe, we could address this observation in more detail.

The improvement in emission uniformity from individual tips and between tips in an array as a result of Ne and Xe cathode bombardment is evident in these investigations. The net apparent smoothing effect due to the removal of protuberances by inert gas ion bombardment that we have observed in our experiments is undoubtedly related to the phenomenon of electrode "conditioning" of high-voltage gaps. In this process the voltage hold-off capability can be increased following low-energy ion bombardment from glow discharges.[15] This increase in breakdown strength is most likely due, at least in part, to the removal of field-enhancing protuberances on the electrode surfaces, leading to locally enhanced field-electron emission (from the cathode) and eventually a vacuum arc.

V. CONCLUSIONS

Hydrogen plasma treatment in conjunction with neon and xenon ion bombardment leads to a significant enhancement in the electron-emission uniformity for each tip and between tips in the array. The effect of the ion bombardment is a net smoothing of the emitter tip surfaces by low-energy sputtering. The process tends to bring the emitter tips to a similar shape by mild sputtering, as tips having greater field enhancement factors are blunted faster than those having a lower enhancement factor, thereby allowing an equilibrium size/shape to be approached. Under our experimental conditions the best results were obtained with Ne. Helium has little effect on the uniformity and with Xe bombardment, leakage and emitter tip destruction are prevalent .

These processes can be readily implemented in technological tube applications as they may be performed *in situ* prior to tube seal-off.

ACKNOWLEDGMENTS

The authors acknowledge helpful discussions with I. Brodie and C.E. Holland during the course of this work. In addition, we thank B.V. Conroy of SRI's glassblowing shop for his assistance in equipment construction and the members of the Vacuum Microelectronics Group—D.A. Thibert, S. Chhokar, S. Shepherd, and L. Wachsman—for emitter tip fabrication. This work was supported by the Advanced Research Projects Agency under Contract No. MDA972-91-C-0029.

REFERENCES

[1]I. Brodie and C.A. Spindt, in *Advances in Electronics and Electron Physics*, edited by P.W. Hawkes (Academic Press, New York, 1992), Vol. 83, Chap. 1, pp. 2–95.

[2]R.H. Fowler and L.W. Nordheim, Proc. Roy. Soc. (London) A **119**, 173 (1928).

[3]R. Gomer, *Field Emission and Field Ionization* (Harvard University Press, Cambridge, MA, 1961).

[4]G.A. Somorjai, *Chemisry in Two Dimensions: Surfaces* (Cornell University Press, Ithaca, NY, 1981).

[5]P.R. Schwoebel and C.A. Spindt, Appl. Phys. Lett. **63**, 33 (1993).

[6]J.A. Stratton, *Electromagnetic Theory* (McGraw-Hill, New York, 1941).

[7]M.K. Miller and G.D.W. Smith, *Atom Probe Microanalysis: Principles and Applications to Materials Problems* (Materials Research Society, Pittsburgh, PA, 1989).

[8]A. von Engel, *Ionized Gases* (Oxford University Press, London, 1955).

[9]L.B. Loeb, *Fundamental Processes of Electrical Discharge in Gases* (Wiley, New York, 1939).

[10]S. Dushman, *Scientific Foundations of Vacuum Technique* (Wiley, New York, 1962).

[11]M. Kaminsky, *Atomic and Ionic Impact Phenomena on Metal Surfaces* (Academic Press, New York, 1965).

[12]H.H. Andersen and H.L. Bay in *Sputtering by Particle Bombardment I*, edited by R. Behrisch (Springer, New York, 1981).

[13]R. Gomer, R. Wortman, and R. Lundy, J. Chem. Phys. **26**, 1147 (1956).

[14]R. Smoluchowski, Phys. Rev. **60**, 661 (1941).

[15]R.V. Latham, *High Voltage Vacuum Insulation: The Physical Basis* (Academic Press, New York, 1981).

TABLES

Table 1

Gas	V_0 (volts)	λ (cm)	$E_{Average}$ (eV)	D_{Total} (Ions/cm^2)	Y_{max} (atoms/cm^2)	$E_{threshold}$ (eV)
H_2	275	9.3×10^{-3}	H_2^+ 36	10^{18}	1×10^{13}	~75
H_2 + 10% He	300	6.0×10^{-3}	He^+ 25	10^{18}	2×10^{15}	~48
H_2 + 10% Ne	300	3.0×10^{-3}	Ne^+ 13	10^{18}	3×10^{16}	~30
H_2 + 10% Xe	450	8.0×10^{-4}	Xe^+ 25	10^{18}	7×10^{16}	~48

FIGURE CAPTIONS

FIG. 1. A schematic of the field-emitter array. The base is single-crystal silicon and the field-emitter cathodes and gate film are vapor-deposited molybdenum. The insulating layer is thermally grown SiO_2.

FIG. 2. Fowler-Nordheim data showing the effect of pure hydrogen and hydrogen + 10% neon plasma treatment on a 127-tip field-emitter array. Line A: FN data prior to hydrogen plasma treatment. Line B: FN data following hydrogen plasma treatment (dose $\sim 1 \times 10^{18}$ ions/cm^2). Line C: FN data following hydrogen + 10% neon plasma treatment (total dose $\sim 2 \times 10^{19}$ ions/cm^2).

FIG. 3. Field electron micrographs corresponding to the FN data shown in Figure 2. (a) Electron micrograph of the 127-tip array prior to hydrogen plasma treatment (V = 147 V, I = 1 μA). (b) Electron micrograph of the array following hydrogen plasma treatment (V = 107 V, I = 1 μA). (c) Electron micrograph of the array following hydrogen + 10% neon plasma treatment (V = 120 V, I = 1 μA).

FIG. 4. Fowler-Nordheim data showing the effect of pure hydrogen and hydrogen + 10% neon plasma treatment on a microfabricated single-tip field emitter. Line A: FN data prior to hydrogen plasma treatment. Line B: FN data following hydrogen plasma treatment (dose $\sim 1 \times 10^{18}$ ions/cm^2). Line C: FN data following hydrogen + 10% neon plasma treatment (total dose $\sim 1 \times 10^{18}$ ions/cm^2). Line D: FN data following an additional hydrogen + 10 % neon dose of 7×10^{18} ions/cm^2.

FIG. 5. Field electron micrographs corresponding to the FN data shown in Figure 4. (a) Electron micrograph, corresponding to curve A in Figure 4, of the single tip prior to

hydrogen plasma treatment (V = 175 V, I = 1 μA). (b) Electron micrograph of the tip following hydrogen plasma treatment, curve B, Figure 4 (V = 133 V, I = 1 μA). (c) Electron micrograph of the single tip following hydrogen + 10% neon plasma treatment, curve D, Figure 4 (V = 130 V, I = 1 μA).

FIG. 6. Fowler-Nordheim data showing the effect of pure hydrogen and hydrogen + 10% xenon plasma treatment on a microfabricated single-tip field emitter. Line A: FN data prior to hydrogen plasma treatment. Line B: FN data following hydrogen plasma treatment (dose ~ 1×10^{18} ions/cm^2). Line C: FN data following hydrogen + 10% xenon plasma treatment (total dose ~ 5×10^{16} ions/cm^2)..

FIG. 7. Field electron micrographs corresponding to the FN data shown in Figure 6. (a) Electron micrograph of the single tip prior to hydrogen plasma treatment (V = 116 V, I = 0.2 μA). (b) Electron micrograph of the tip following hydrogen plasma treatment (V = 192 V, I = 0.2 μA). (c) Electron micrograph of the single tip following hydrogen + 10% xenon plasma treatment (V = 128 V, I = 0.2 μA).

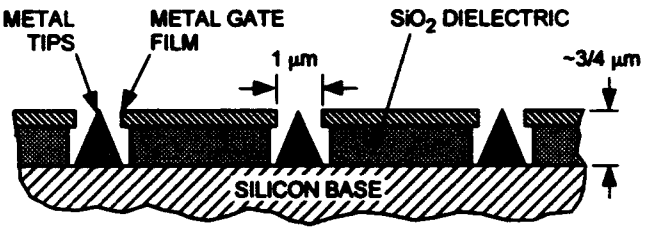
METAL TIPS
METAL GATE FILM
1 μm
SiO_2 DIELECTRIC
~3/4 μm
SILICON BASE
sc-021193-jd

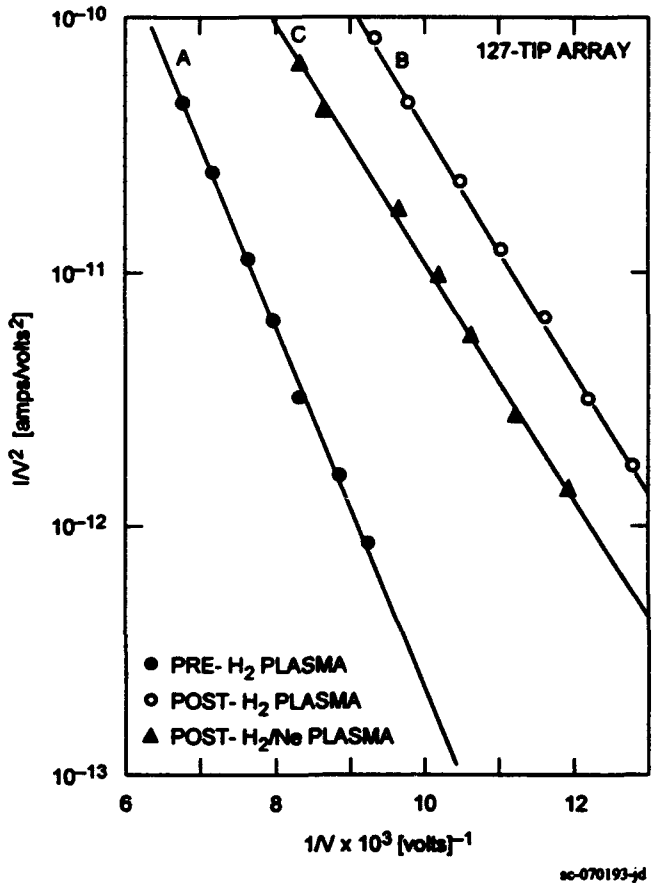
127-TIP ARRAY
A
B
C
10^{-10}
10^{-11}
10^{-12}
10^{-13}
I/V^2 [amps/volts^2]
6
8
10
12
1/V x 10^3 [volts]$^{-1}$
● PRE- H_2 PLASMA
○ POST- H_2 PLASMA
▲ POST- H_2/Ne PLASMA
sc-070193-jd

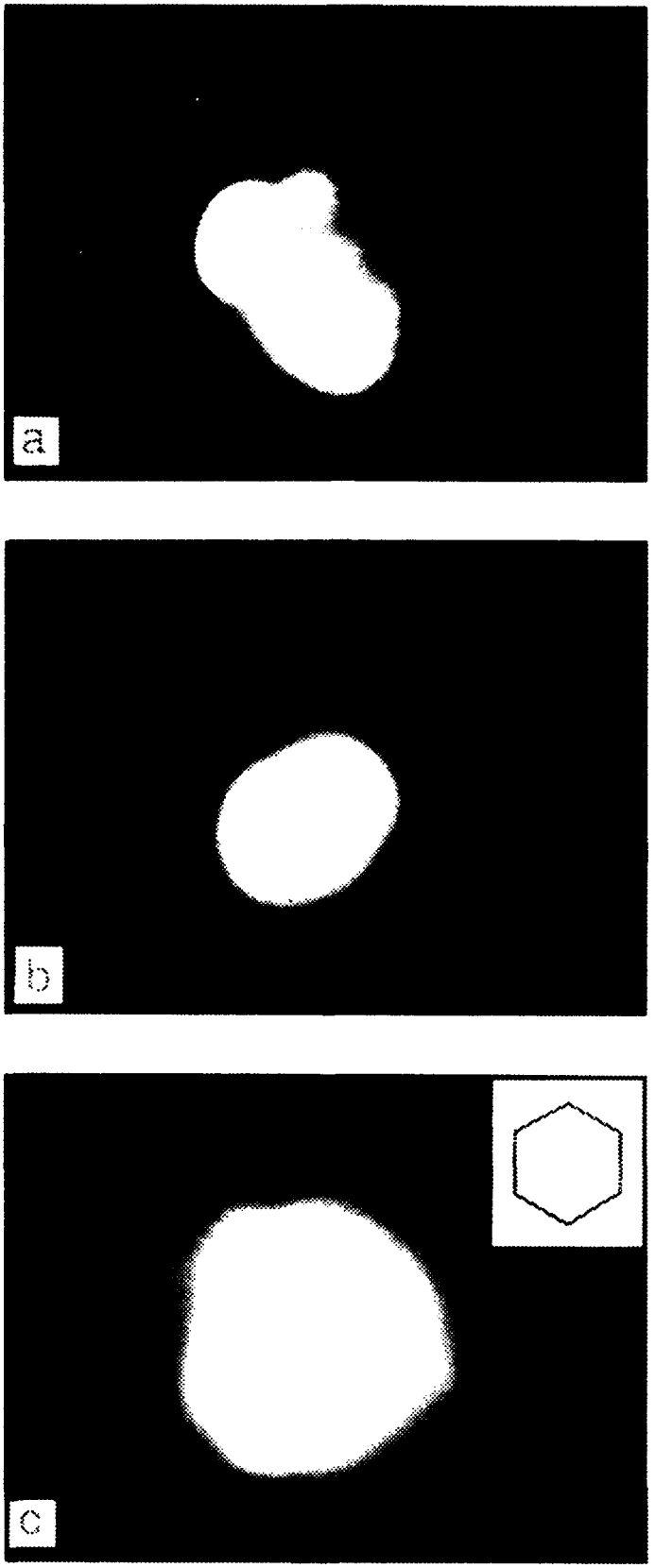

sp-652094-ad

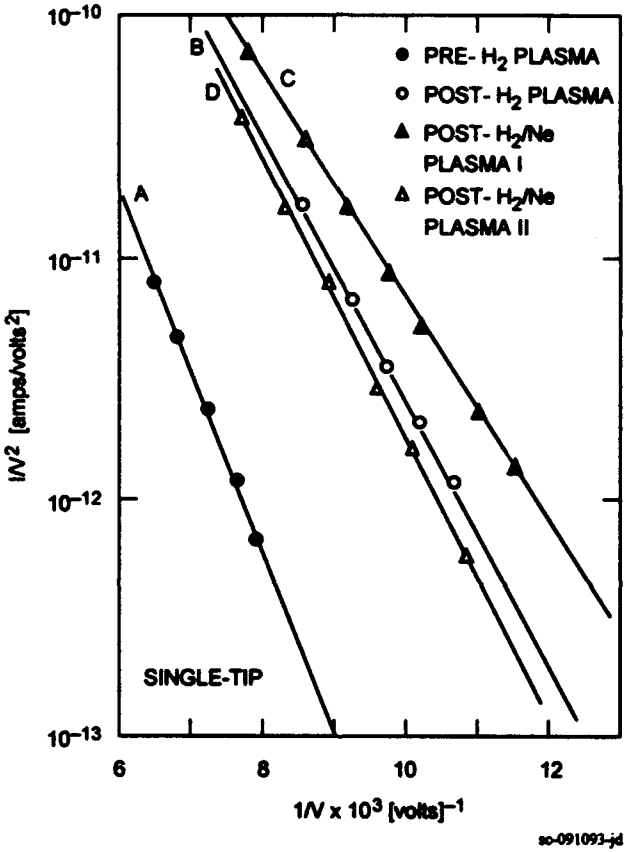
10^{-10}
10^{-11}
10^{-12}
10^{-13}
I/V^2 [amps/volts^2]
6
8
10
12
1/V x 10^3 [volts]$^{-1}$
A
B
C
D
PRE- H_2 PLASMA
POST- H_2 PLASMA
POST- H_2/Ne PLASMA I
POST- H_2/Ne PLASMA II
SINGLE-TIP
so-091093-jd

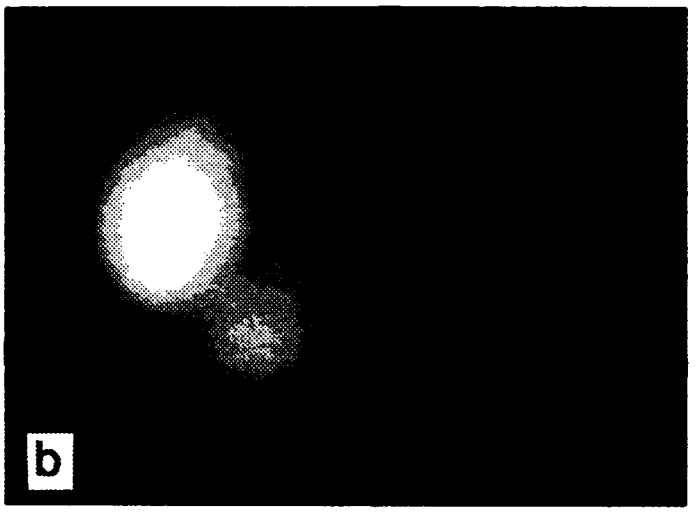

sp-752094-ed

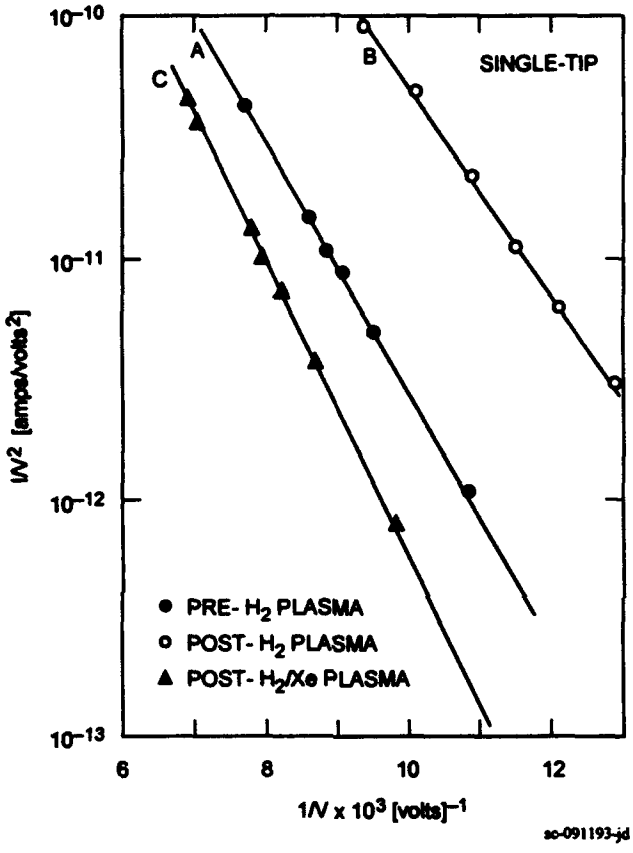
10^{-10}
10^{-11}
10^{-12}
10^{-13}
I/V^2 [amps/volts^2]
A
B
C
SINGLE-TIP
PRE- H_2 PLASMA
POST- H_2 PLASMA
POST- H_2/Xe PLASMA
6
8
10
12
$1/V \times 10^3$ [volts]$^{-1}$
sc-091193-jd

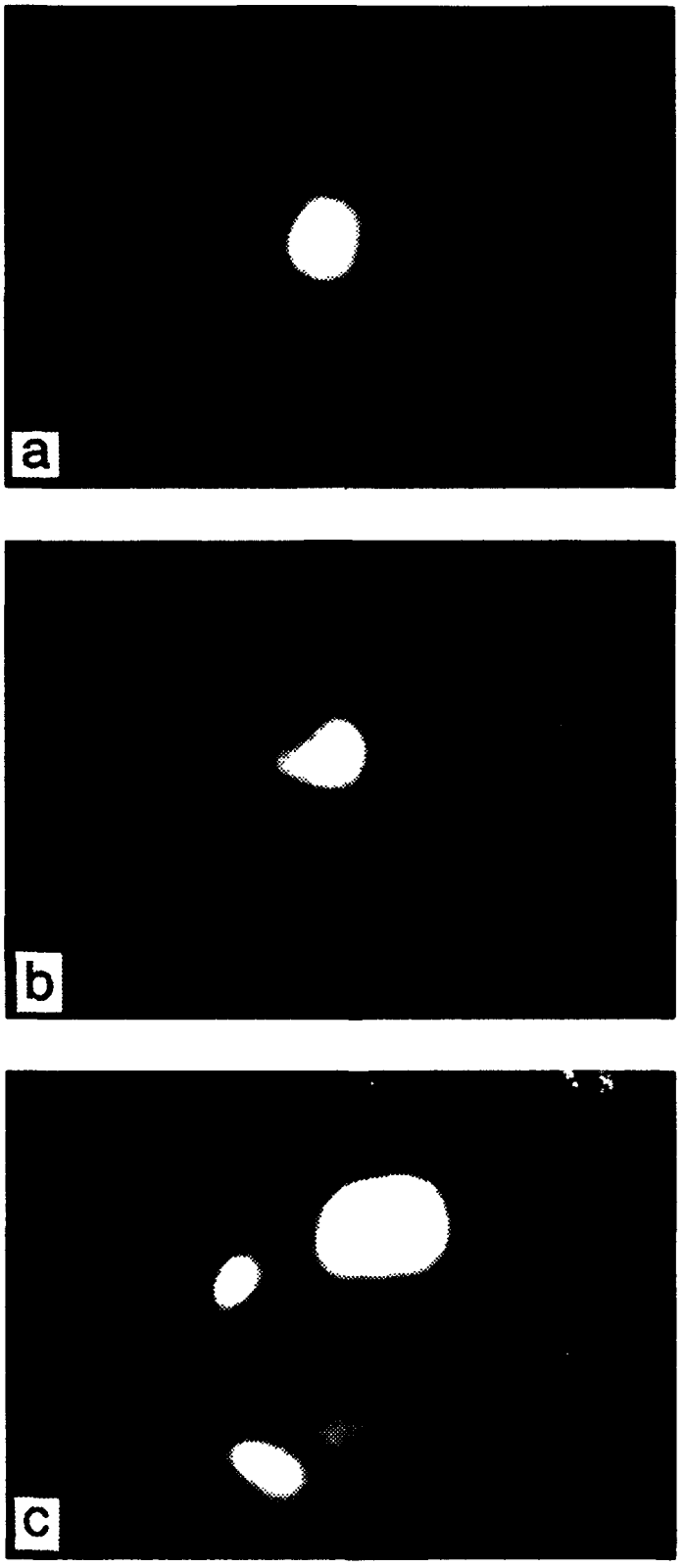

sp-852094-ad